MISSOURI COOPERATIVE HIGHWAY RESEARCH PROGRAM
REPORT **68-14**

STUDY OF A PRECAST-PRESTRESSED MODEL BRIDGE SLAB

MISSOURI STATE HIGHWAY DEPARTMENT
UNIVERSITY OF MISSOURI - COLUMBIA
BUREAU OF PUBLIC ROADS

STUDY OF A PRECAST-PRESTRESSED MODEL BRIDGE SLAB

Prepared for

MISSOURI STATE HIGHWAY DEPARTMENT

by

JOHN R. SALMONS

and

SHAHROKH MOKHTARI

DEPARTMENT OF CIVIL ENGINEERING

UNIVERSITY OF MISSOURI

COLUMBIA, MISSOURI

in cooperation with

U.S. DEPARTMENT OF TRANSPORTATION

FEDERAL HIGHWAY ADMINISTRATION

BUREAU OF PUBLIC ROADS

ABSTRACT

A half-scale concrete composite model bridge slab is studied to evaluate the structural performance of a 36-foot long, two-lane, highway bridge span. The proposed composite member is composed of a prestressed concrete channel, an interior void form, and a top slab of cast-in-place concrete. A theoretical analysis of the load distribution behavior of an orthotropic plates based on the Guyon-Massonnet distribution theory is presented. Application of the theory to this particular bridge system together with a sample calculation is presented in an appendix.

An 18-foot long, 12'6" wide model bridge span consisting of five prestressed channels and a cast-in-place top slab was constructed for the purpose of experimental varification of the analytical analysis.

Two series of tests were conducted in this study. In the first series of tests a single concentrated load was applied to a grid of 30 load points. The load distribution behavior was studied in terms of the distribution pattern of the measured deflections.

In the second series of tests a simulated S16 trailer load was applied to the two-lane model bridge slab. The wheel load distribution, the ultimate behavior of the system, and the failure mode were investigated. Complete composite action was observed through the test and the failure resulted from compression crushing of the top slab in the vicinity of the load line.

TABLE OF CONTENTS

CHAPTER PAGE

LIST OF FIGURES

FIGURE PAGE

LIST OF TABLES

TABLE PAGE

CHAPTER I

INTRODUCTION

1.1 GENERAL

A particular type of prestressed-precast composite system has been proposed for use in highway bridge construction. The proposed bridge system consists of a number of prestressed concrete channels placed side by side with a continuous cast-in-place top slab. A series of 36 foot long, single units composed of a channel, an interior void, and a concrete top slab were designed, fabricated, and tested in the Department of Civil Engineering, University of Missouri at Columbia to study the behavior of the bridge members[1].*

To evaluate the structural performance of the proposed bridge system, an additional experimental study was carried out on a bridge span composed of this type member. Due to limited laboratory facilities, a one-half scale model bridge span consisting of five prestressed channels and a continuous cast-in-place top slab was constructed to simulate a 36-foot long, two lane, highway bridge span.

Structural similarity between the model members and the corresponding prototypes has been investigated in a separate study[2], where a series of single unit model members were tested and the accuracy of the theoretical similitude relations were examined. It was found that the structural behavior of a full-scale member can be predicted by tests on models utilizing the proper scale factors.

---

*Superscripts refer to entries in the bibliography.

Based on the similitude findings, test results of the one-half scale model bridge span represent the behavior of a full scale bridge slab. Test data were adjusted, wherever necessary, utilizing the proper scale factor.

1.2 LITERATURE SURVEY

One of the most important design criteria in composite concrete bridges is load distribution i.e., the manner in which a loaded member transfers part of the applied external load to the adjacent members. Several theoretical approaches have been presented by a number of investigators[3,4]. However, the first practical approach suitable for design was introduced by a French Engineer, Guyon, in 1946. This method was further extended by Massonnet in 1950. Work of these two investigators has been introduced in English literature by P.B. Morice and G. Little [5]. In this method, a multi-unit structure was transformed into an elastic orthotropic plate whereby customary plate solutions were utilized to obtain certain distribution coefficients. These coefficients were simply the ratio of the deflection of a certain point on the plate under action of concentrated force to the mean deflection of the plate under uniform load. Furthermore, the authors presented a series of design curves which gave the proper distribution coefficients for any known set of flexural and torsional stiffnesses and given load positions. Also, the above approach was examined by the authors through laboratory tests of several multi-beam bridges and satisfactory agreement was observed. The above method was used in the study presented in this paper and will be discussed in the next chapter.

In a series of papers presented by K.S. Rakshit[6], the Guyon-

Massonnet theory and the Morice's distribution curves have been further elaborated. Morice's curves only handle the two extreme cases of no torsional and full torsional rigidity of the bridge grillage. When torsional stiffness of the slab is a fraction of the "full torsion" case, an interpolation approach should be used which is rather lengthy. Rakshit presented a number of curves which give the distribution coefficients for a certain range of values of flexural and torsional stiffnesses without any interpolation process. The author also furnishes some practical examples through which good agreement between his method and Morice's approach was observed. One shortcoming of the simplified method is that the given curves are only valid for certain values of flexural stiffness and no accurate interpolation is possible.

G. Little and R. E. Rowe have reported results of tests performed at the Cement and Concrete Association Laboratories on plastic models of bridges[7]. Two types of sections were investigated, one composed of a continuous slab stiffened with rectangular web in both directions and another composed of cellular sections in both directions. The objects of these tests were to determine the effective value of torsional stiffness of those types of bridges consistent with the assumptions of the Guyon-Massonnet theory. The theory, as shown by Massonnet, requires that the torsional stiffness of the slab to be used in the analysis should not be in proportion to the real value, $\frac{h^3}{3}$, but half this value $\frac{h^3}{6}$, where h is the thickness of the slab. On the other hand, torsional stiffness of the stiffening web of any shape should be calculated by the conventional method. Therefore, the torsional stiffness of the entire composite section is a combination of effects found by adding one half

the torsional stiffness of the slab to the actual torsional stiffness of the stiffening web or stem.

The experimental distribution coefficients were compared with those computed using this approach. In the case of the T beam bridge good agreement was observed. However, in the case of the cellular box section bridge, it was found that satisfactory results could only be obtained by measuring the torsional stiffness of a one-unit box beam experimentally. The authors recommended the use of the Wittrick torsion formula[8]:

$$Gk = \frac{4A^2G}{\oint \frac{ds}{t}}$$

where:

G - The modulus of rigidity

Gk - The torsional stiffness

A - The area of void in the box

S - The distance measured along the inner perimeter

t - The wall thickness

A half-scale model of a precast-prestressed concrete bridge deck continuous over two spans was tested at the Portland Cement Association Laboratory[9]. The model bridge was composed of five pre-stressed I girders in each span with a continuous cast in place top slab. The Guyon-Massonnet load distribution theory was used to predict load transfer characteristics of the bridge under service loads and overloads with deck slab cracked and uncracked. Comparison of experimental and theoretical results showed the following:

1. This type of composite concrete bridge acts essentially elastic when subjected to service loads and even to appreciable overloads.

2. The Guyon-Massonnet theory for load distribution predicted very closely the behavior of the composite bridge even with the top slab cracked and under applied overloads, provided that the appropriate cracked and uncracked stiffnesses are used in distribution predictions. Also, it was noted that the torsional stiffness of the bridge should be accurately taken into account in such predictions.

Lateral distribution of load in a composite box girder bridge, has been investigated by S. B. Johnston and A. H. Mattock[10]. The particular type of section used consisted of trapezoidal section steel girders made composite with a reinforced concrete deck slab. Transverse distribution of deflection and bending moments under application of point loads and AASHO truck loading were compared with theoretical values based on the folded plate theory of Goldberg and Leve[11]. In this theory the first three terms of the Fourier Series representing a concentrated load were used. Results were in close agreement and confirmed the applicability of folded plate theory to this type of bridges. The box girder bridge was found to be more efficient in load transfer than the conventional I girder bridges due to the high torsional stiffness of the closed box sections.

1.3 SCOPE

The object of this study was to investigate the structural performance of the proposed bridge system through tests carried out on a half-scale concrete bridge span simulating a 36-foot, two-lane, highway bridge. Included in this report are the theoretical load distribution

analysis, the experimental load transfer characteristics of the bridge slab under the action of concentrated loads and the comparison between the two sets of data.

In addition, ultimate load capacity and the mode of failure of the bridge model, under the application of simulated wheel loads, are presented.

CHAPTER II

THEORETICAL ANALYSIS

2.1 GENERAL

The general bending theory of orthotropic plates, simply supported on two opposite sides, and the Guyon-Massonnet load distribution theory are briefly summerized. This approach is applied to the particular prestressed-precast composite bridge slab, and the procedure of obtaining the lateral moment and deflection distribution coefficients are outlined.

2.2 ASSUMPTIONS

The theory is developed from two basic assumtions:

1. The actual structure is, for the purpose of calculation, replaced by an elastically equivalent system uniformly distributed in both directions. Thus, the equivalent structure has the same average flexural and torsional stiffnesses everywhere, as the actual bridge.

2. Based on the first assumption, the equivalent structure can be treated as an orthotropic plate, and all the assumptions normally used in the derivation of the plate equation are valid.

2.3 BASIC PRINCIPLES

The problem of bending of orthrotropic plates has been treated by Timoshenko[12] and the deflected shape of such a plate can be expressed by

$$D_x \frac{\partial^4 w}{\partial x^4} + 2H \frac{\partial^4 w}{\partial x^2 \partial y^2} + D_y \frac{\partial^4 w}{\partial y^4} = q \qquad (2.1)$$

where:

$D_x = \frac{E'_x h^3}{12}$ - Flexural stiffness in the x direction

$D_y = \frac{E'_y h^3}{12}$ - Flexural stiffness in the y direction

$H = \frac{h^3}{12}(E'' + 2G)$ - Combined torsional stiffness in both directions

h - Thickness of the slab

E'_x - Effective bending modulus of elasticity in the x direction

E'_y - Effective bending modulus of elasticity in the y direction

E'' - An elastic constant expressing the Poisson's ratio effect in the stiffnesses in both directions

G - Modulus of rigidity

q - Intensity of the load at a point (x, y)

Rigidities D_x, D_y, and H can be determined and have been computed in a few common cases by Timoshenko[12]. If the Poisson's ratio μ is small, which is the case for concrete, E'' can be neglected and equation (2.1) can be simplified.

$$\rho_x \frac{\partial^4 w}{\partial x^4} + (\gamma_x + \gamma_y) \frac{\partial^4 w}{\partial x^2 \partial y^2} + \rho_y \frac{\partial^4 w}{\partial x^4} = q \qquad (2.2)$$

where:

ρ_x, ρ_y - Flexural stiffnesses per unit length

γ_x, γ_y - Torsional stiffnesses per unit length

It is also more convenient to express equation (2.2) in a form involving only flexural stiffnesses:

$$\rho_x \frac{\partial^4 w}{\partial x^4} + 2\alpha\sqrt{\rho_x \rho_y} \frac{\partial^4 w}{\partial x^2 \partial y^2} + \rho_y \frac{\partial^4 w}{\partial y^4} = q \qquad (2.3)$$

where:

$\alpha = \frac{\gamma_x \gamma_y}{2\sqrt{\rho_x \rho_y}}$ is a dimensionless parameter

Equation (2.3) is the general expression for the normal deflection of a general orthotropic plate with general boundary conditions and loading, when the effect of Poisson ratio has been neglected. This equation is the governing equation for distribution theories considered

in this study.

A common case encountered in bridge slabs is a plate simply supported on two opposite edges and free on the other sides similar to that shown in Fig. 2.1. Guyon and Massonnet have treated this case for isotropic and orthotropic plates with or without torsional stiffnesses. Rowe[13], presented the Guyon approach as applied to the case where Poisson's ratio is not negligible.

2.4 GUYON - MASSONNET SOLUTION

Consider the simply supported plate in Fig. 2.1 with a load distribution in any manner, not necessarily sinusoidal as shown, along an eccentrict strip. Guyon showed that the load function can be expressed in Fourier series:

$$q = \sum_{m=1}^{\infty} \frac{Am}{b} \sin \frac{m\pi x}{L} \{\tfrac{1}{2} + \sum_{n=1}^{\infty} \cos \frac{n\pi}{b} (y-e)\}$$

or

$$q = \sum_{m=1}^{\infty} f(x) + \sum_{m=1}^{\infty} \sum_{n=1}^{\infty} f(x,y)$$

As a result equation (2.3) can be separated into two parts:

$$(a) \quad \rho_x \frac{\partial^4 w_1}{\partial x^4} + 2\alpha \sqrt{\rho_x \rho_y} \frac{\partial^4 w_1}{\partial x^2 \partial y^2} + \rho_y \frac{\partial^4 w_1}{\partial y^4} = \sum_{m=1}^{\infty} f(x)$$

$$(b) \quad \rho_x \frac{\partial^4 w_2}{\partial x^4} + 2\alpha \sqrt{\rho_x \rho_y} \frac{\partial^4 w_2}{\partial x^2 \partial y^2} + \rho_y \frac{\partial^4 w_2}{\partial y^4} = \sum_{m=1}^{\infty} \sum_{n=1}^{\infty} f(x,y)$$

and the actual deflection of the plate will be $w = w_1 + w_2$. The solution to equation (a) can be expressed as a function of x only

$$w_1 = \sum_{m=1}^{\infty} B_m \sin \frac{m\pi x}{L} \quad \text{where,} \quad B_m = \frac{L^4 A_m}{m^4 \pi^4 \rho_x}$$

which satisfies the boundary conditions. Every term of this series represents the deflection produced if the m th term of the load series is

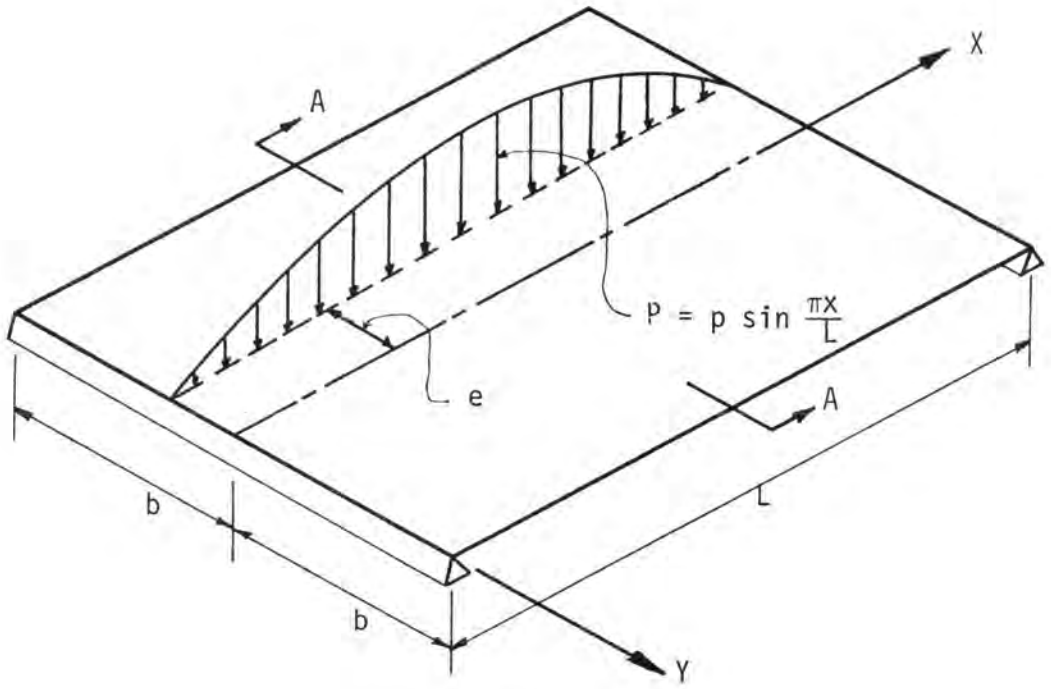

Fig. 2.1 Sinusoidal Line Load on the Equivalent Bridge

distributed uniformly over the entire transverse section of the plate. It may be defined as "mean deflection" W

$$W = \sum_{m=1}^{\infty} W_m \quad ; \quad W_m = B_m \sin \frac{m\pi x}{L} \tag{2.4}$$

To obtain a solution to (b), a Levy series solution is adopted.

$$w_2 = \sum_{m=1}^{\infty} Y_m C_m \sin \frac{m\pi x}{L}$$

Substituting this solution in equation (b), the following ordinary differential equation can be obtained;

$$m^4\theta^4 Y_m - \frac{2\alpha m^2\theta^2 b^2}{\pi^2} Y_m^{11} + \frac{b^4}{\pi^4} Y_m^{1V} = \sum_{n=1}^{\infty} \cos \frac{n\pi}{b} (y-e)$$

where:

$$\theta = \frac{b}{L} \sqrt[4]{\frac{\rho_x}{\rho_y}}$$

$$C_m = \frac{b^4}{\pi^4} \frac{A_m}{b}$$

The solution to this equation consists of two parts, the particular and the complementary solutions. The operation is lengthy and will not be presented here.

The sum of the solutions of equations (a) and (b), $w = w_1 + w_2$ is:

$$w = \sum_{m=1}^{\infty} B_m \sin \frac{m\pi x}{L} \{1 + 2m^4\theta^4 y_m\}$$

Taking the quantity in bracket as k_m and using equation (2.4):

$$w = \sum_{m=1}^{\infty} W_m k_m \tag{2.5}$$

where k_m is a constant for every value of m.

Therefore:

$$w = k_1 W_1 + k_2 W_2 + \ldots + k_m W_m$$

$$W = W_1 + W_2 + \ldots + W_m \quad \text{i.e., equation (2.4)}$$

$$K = \frac{w}{W} = \frac{k_1 W_1 + k_2 W_2 + \ldots + k_m W_m}{W_1 + W_2 + \ldots + W_m}$$

where K is the true distribution coefficient. It is also noted that W_m is inversely proportional to m^4 and the above expression rapidly converges and for practical purposes only the first term may be retained or:

$$K \simeq \frac{w_1}{W_1} = k_1 \qquad (2.6)$$

It should be noted that the above distribution coefficient also applies to the longitudinal bending moments, though in the latter case the approximation is not accurate since the differential equation for bending moment is of second order. Thus the series containing "mean bending moment" is inversely proportional to m^2 and convergence is slower. Guyon suggested that to allow for the approximation in taking only the first term the theoretical moment found from the expression

$$M_x = M_{mean}\, k_1 \qquad (2.7)$$

should be increased by 10 to 15 percent to give the actual moment.

2.5 PHYSICAL MEANING OF K COEFFICIENTS

Referring again to equation 2.6 it is noted that w_1 is the deflection of a point on the bridge when m =1, i.e. when only one term of the load Fourier Series and only one term of the deflection Levy Series are considered. This in fact would mean that the load applied to the bridge is a sinesoidal line load in the x direction at some eccentricity e from x-axis as shown in Fig. 2.1.

Furthermore, W_1 is the "mean deflection" when m = 1. If, at the point under consideration, the magnitude of the sinusoidal line load is distributed uniformly across the width of the bridge the

deflection of the bridge will be constant just as that of a simply supported beam. This deflection is considered to be the "mean deflection".

The distribution coefficient is therefore the ratio of the vertical deflection, w_1, of a point on the bridge under the effect of a sinusoidal line load, to the deflection of the same point when the load is distributed uniformly over the entire width of the bridge. This is illustrated in Fig. 2.2.

It is obvious that the primary interest of a designer is to know how much of the load applied to the bridge is carried by each longitudinal girder, or what share of the bending moment is resisted by each girder. As a result, longitudinal girders could be more efficiently designed for the load and moment actually carried by each member. Obviously, the portion of load carried by every girder depends on the position and manner of distribution of load along the width of bridge. For instance, when the load is uniformly distributed over the entire width, all girders carry equal share of the load. From the above theory it is realized that knowing the distribution coefficient at any point and the mean deflection or moment, the actual moment, deflection or load at that point can be determined.

As mentioned previously, the composite model bridge slab considered in this study consisted of five prestressed channels with a continuous concrete top slab as shown in Fig. 2.3. It was more convenient to consider the bridge slab as five composite box members connected together by means of the continuous top slab. In addition, for the purpose of the load transfer study, only the deflections and moments at the centerline of these five box members were considered. With reference to Fig. 2.4, if a

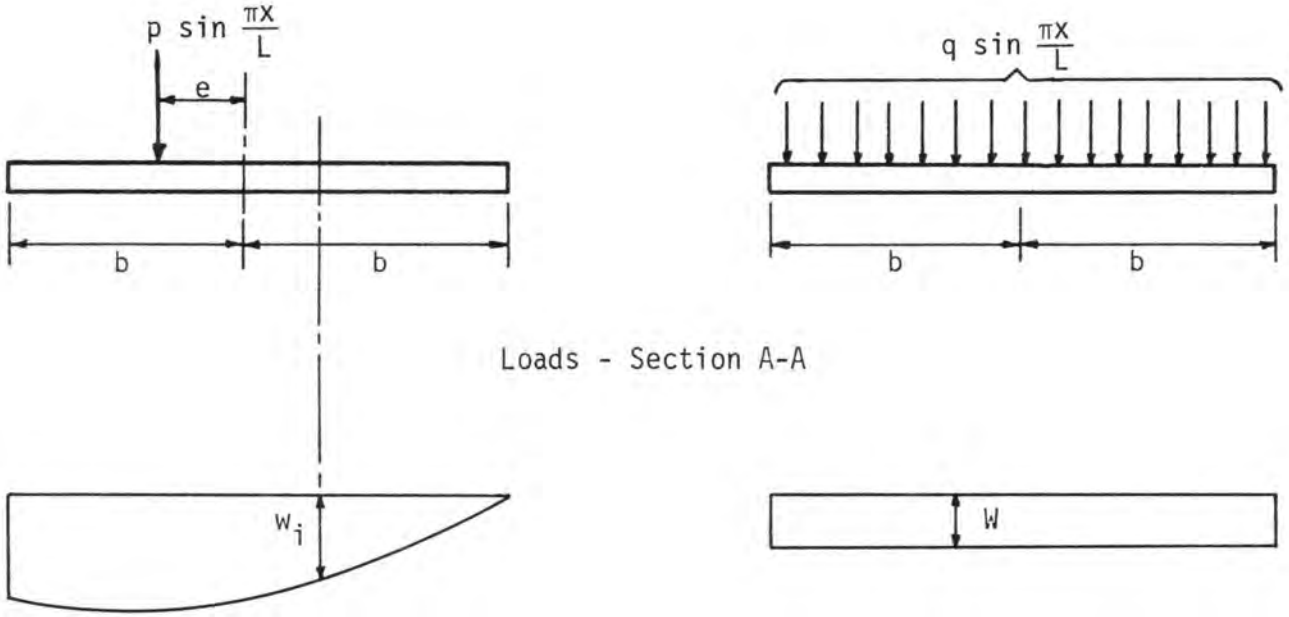

$$K_i = \frac{w_i}{W}$$

Fig. 2.2 Physical Meaning of Distribution Coefficient K

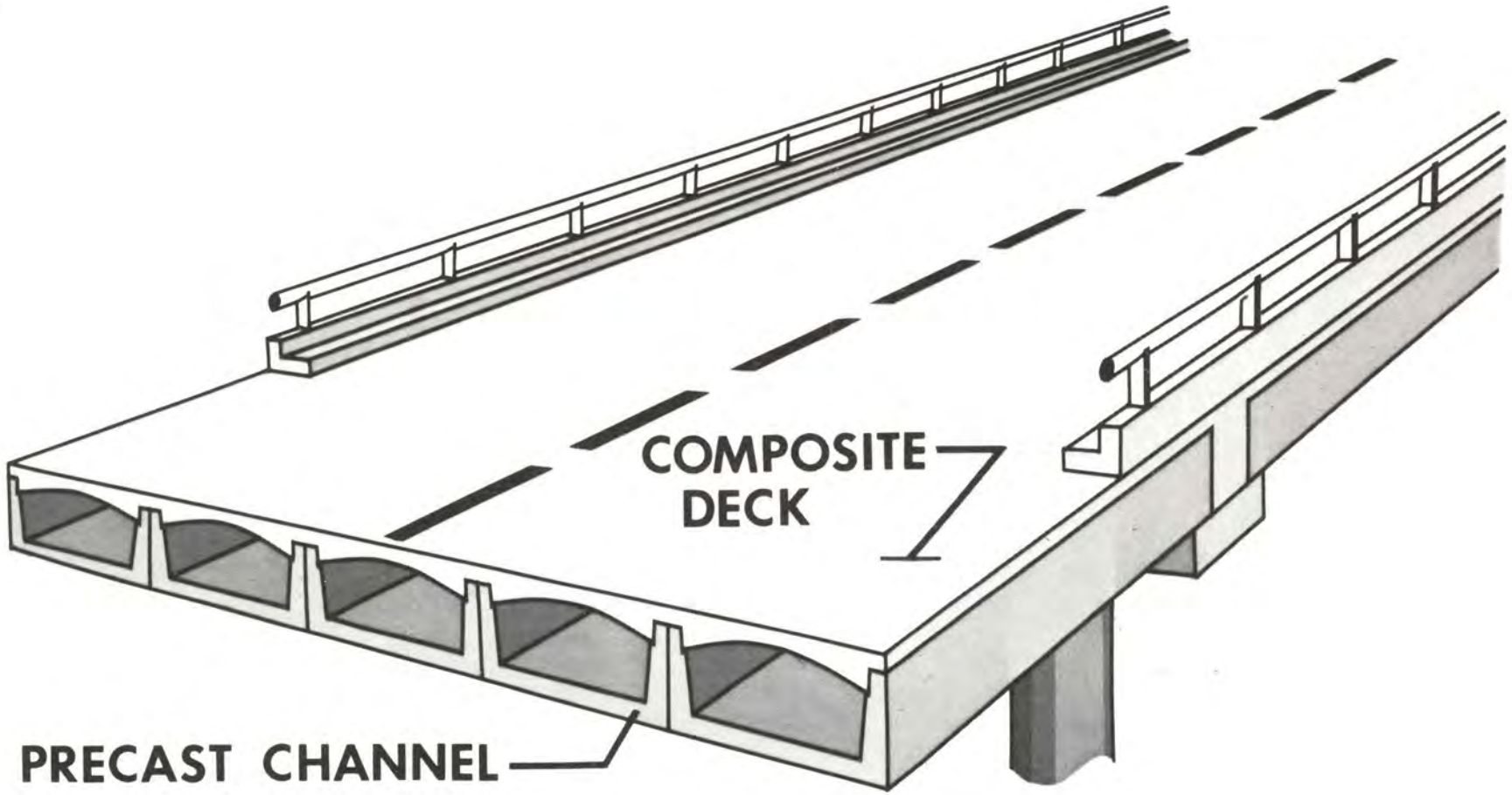

Fig. 2.3 Pictorial View of the Prestressed-Precast Composite Bridge

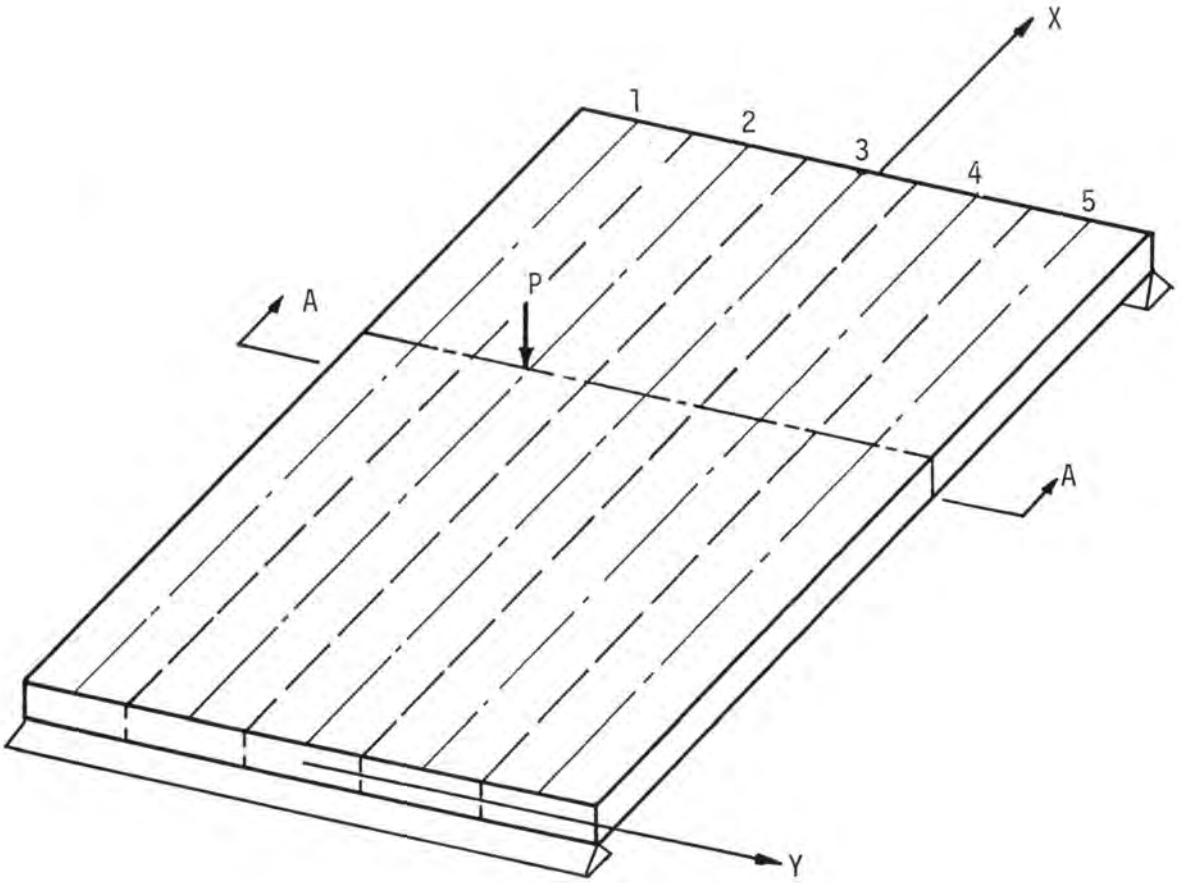

Load Location

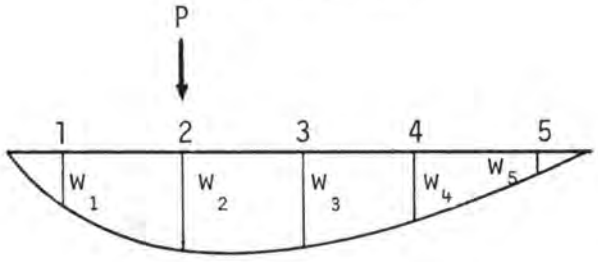

Deflected Surface

Fig. 2.4 A Five Member Bridge Under Eccentric Load P

concentrated load P is applied at the center line of box number 2, then, based on the above theory, at section A the deflection of every member will be equal to the corresponding distribution coefficient multiplied by the mean deflection:

$$w_i = W_1 K_i$$

and the sum of the deflections of all the five members would be:

$$W = W_1 (K_1 + K_2 + K_3 + K_4 + K_5).$$

The percentage of the sum of the deflections carried by each member will be

$$\frac{W_1 K_i}{W_1 (K_1 + K_2 + K_3 + K_4 + K_5)} (100)$$

or

$$\frac{K_i (100)}{K_1 + K_2 + K_3 + K_4 + K_5}.$$

Therefore, it is possible to compare the experimental data with Guyon-Massonnet distribution factors directly without involving the mean deflection. This is accomplished by measuring the actual deflection of each member under the applied load and comparing these values. This is done without losing the physical sense of load distribution since the sum of the deflections or the total bending moment of the five members represents the total external load or the total applied bending moment.

2.6 SUMMARY OF THE METHOD

Summarizing the foregoing discussion it can be noted that the value of the distribution coefficient K depends on:

1. The value of a certain flextural stiffness parameter, θ is given by $\theta = \frac{b}{L} \sqrt[4]{\frac{\rho_x}{\rho_y}}$

where b and L are shown in Fig. 2.1.;

2. The value of the torsional stiffness parameter α given by

$$\alpha = \frac{\gamma_x + \gamma_y}{2\sqrt{\rho_x \rho_y}};$$

3. The eccentricity, e, of the line load from the x-axis;

4. The ordinate y of the point on the bridge under consideration.

In order to obtain the distribution coefficient K for a given bridge slab, the following steps are necessary:

1. Compute α and θ from the given stiffnesses;
2. For a given load position, i.e. given e, refer to Guyon distribution curves for $\alpha = 1$ as given by Morice and Little[5];
3. Obtain the K coefficient for all the longitudinal members of the bridge for $\alpha = 0$ and $\alpha = 1$ designated as K_0 and K_1 respectively;
4. Use the following interpolation formula to obtain K factor for the particular α of the bridge

$$K_\alpha = K_0 + (K_1 - K_0)\sqrt{\alpha}.$$

The above procedure and the necessary computations for obtaining the K coefficients of the particular model Slab studied in this report are given in greater detail in Appendix A.

CHAPTER III

FABRICATION AND TESTING PROCEDURES

3.1 FABRICATION

Five prestressed concrete channels were constructed in the Civil Engineering Laboratory at the University of Missouri. A detailed description of the construction method, curing procedure, and the particular dimensions of thse members has been presented elsewhere[2]. After on average curing period of six months these channels were moved to the testing site and placed on concrete piers as shown in Fig. 3.1. Corrogated metal sheets bent into arches were placed in the channels, as shown in Fig. 3.2, to form the required void space. Top slab reinforcement consisted of longitudinal #3 bars at about 7" spacing over each channel and tranverse reinforcement consisted of #4 bars at 6" spacing along the entire span. The transverse reinforcement was designed by considering a one-foot strip of top slab in the transverse direction acting as a continuous beam with channel legs as the intermediate supports. Maximum design moment due to truck loading was obtained by means of moment distribution.

Two types of shear connectors were used as shown in Fig. 3.3. The shear connectors were welded to the 1/2" angles embedded in the channel legs. These angles were in turn welded to #3 bars extended in the channel as shown in Fig. 3.3, and were placed prior to casting of the prestressed channels.

Fig. 3.1 Precast Units over the Supports

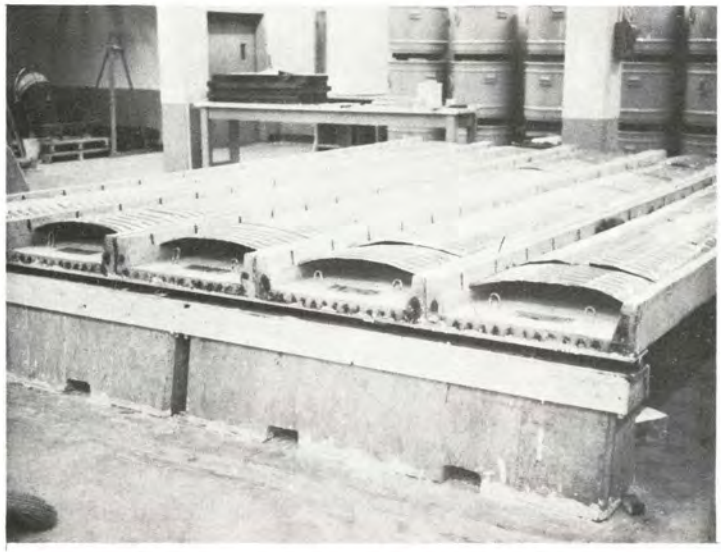

Fig. 3.2 Void Form in Place

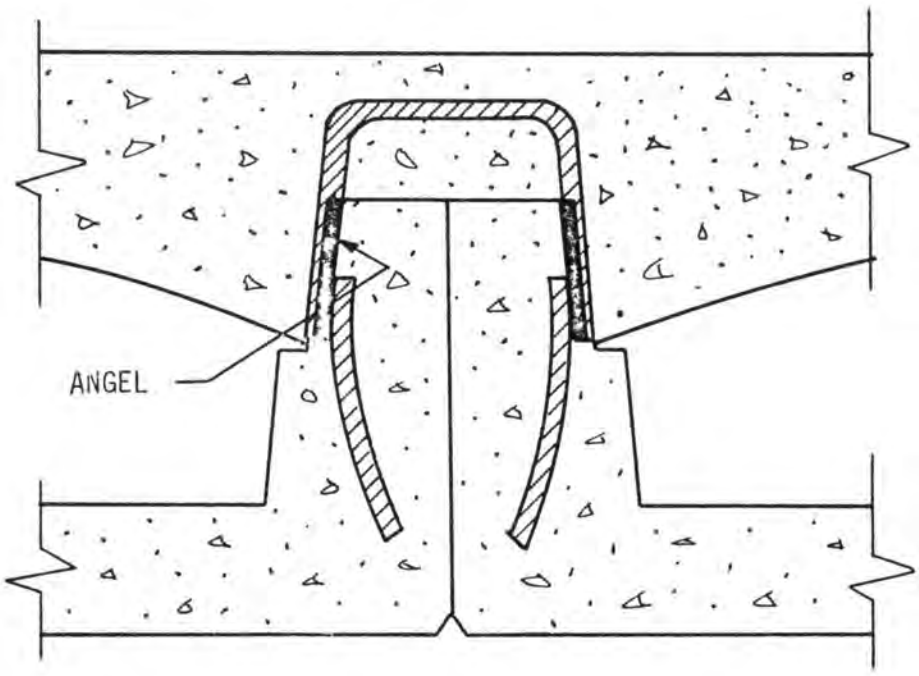

At interior joint

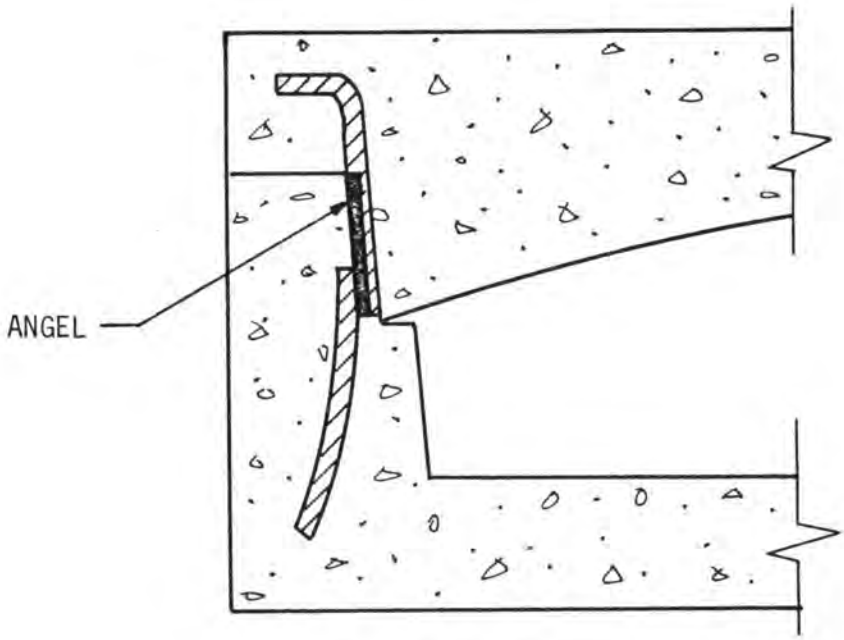

At exterior joint

Fig. 3.3 Shear Connector Detail

After casting the top slab, wet curing was maintained for 10 days followed with approximately two months of normal curing conditions. The overall dimensions of the model bridge span were 18 feet long, 12.5 feet wide and 9" deep.

3.2 INSTRUMENTATION

The composite bridge slab was instrumented to measure deflection, strains, slip and separation at the interface of the two composite components.

Strain meters with a 6" gage length were attached to the top slab, the bottom and both sides of the composite member as shown in Fig. 3.4. On the top surface these meters were placed at the channel joints, and on the bottom surface they were attached to the channel on each side of the joint line.

In order to measure any possible slip or separation at the composite interface dial gages were attached to the slab on the top surface and both sides as shown in Fig. 3.4 parts (1) and (2). On the top surface a number of holes were drilled until the top surfaces of the channel legs were reached. Smaller concentric holes were drilled in the channel legs and steel rods were bonded in these holes. Horizontal and vertical motions of this rod were measured by dial gages as the slip and separation, respectively. Fig. 3.5 shows a pair of dial gages mounted next to the rod and Fig. 3.6 shows a pair of slip and separation gages on one side of the slab.

During the first testing phase the deflection of each box unit was measured at the midspan by deflectometers beneath the bridge slab. In

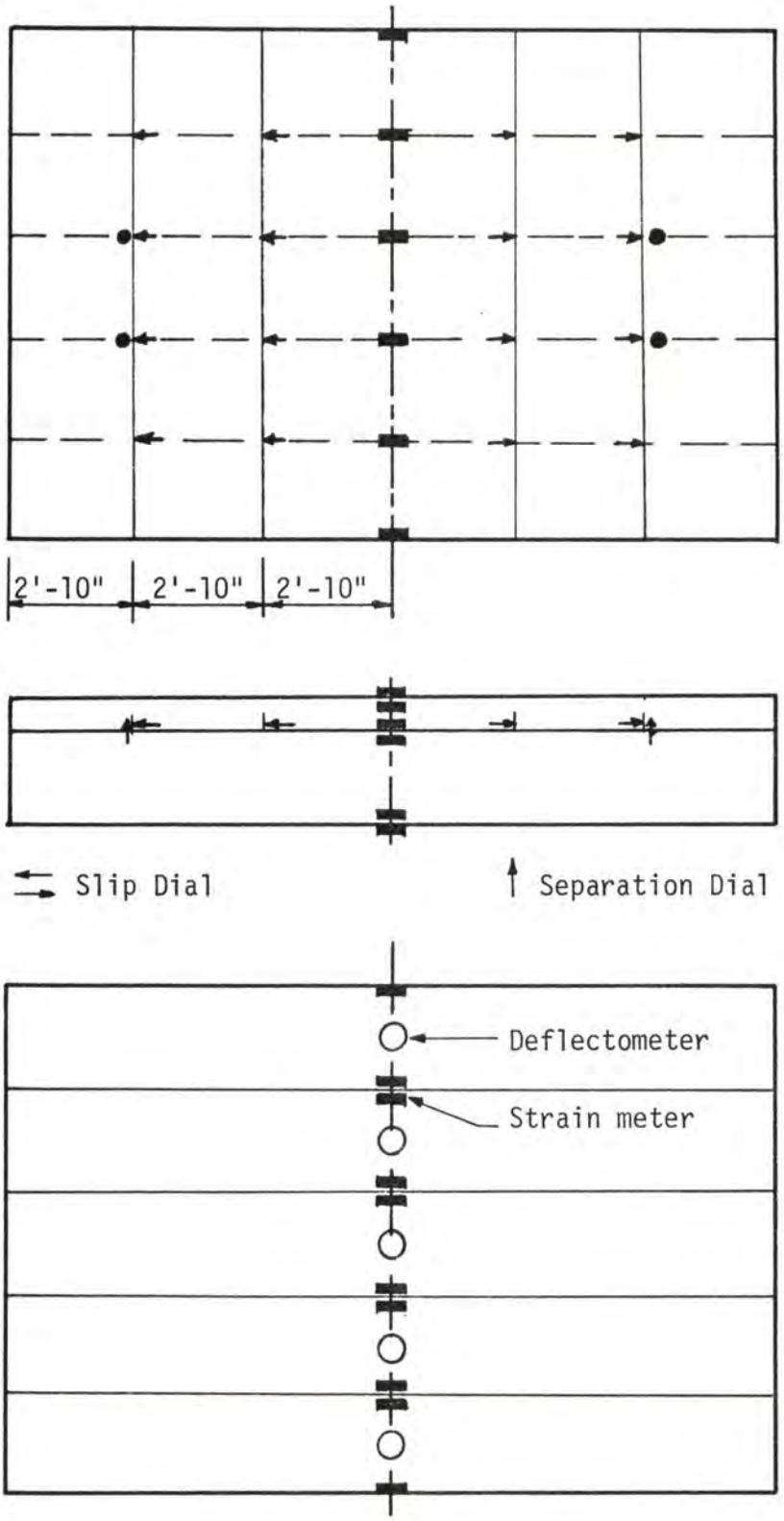

Fig. 3.4 Instrumentation: Top, Side, Bottom Views

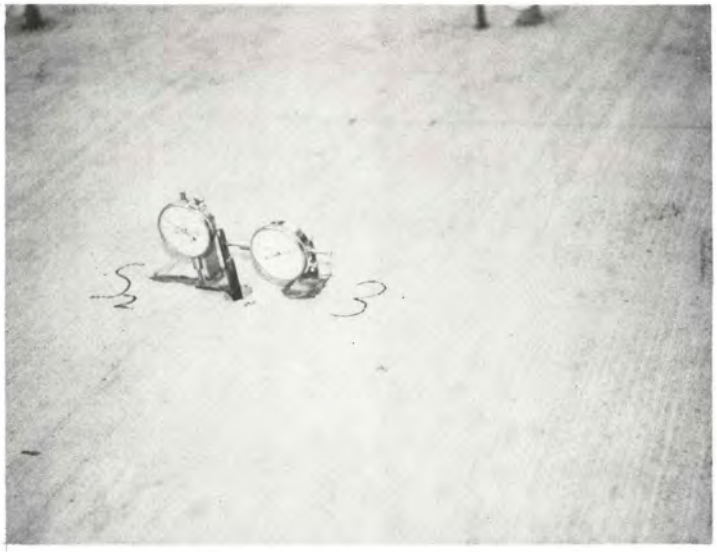

Fig. 3.5 Slip and Separation Dials on the Top Surface

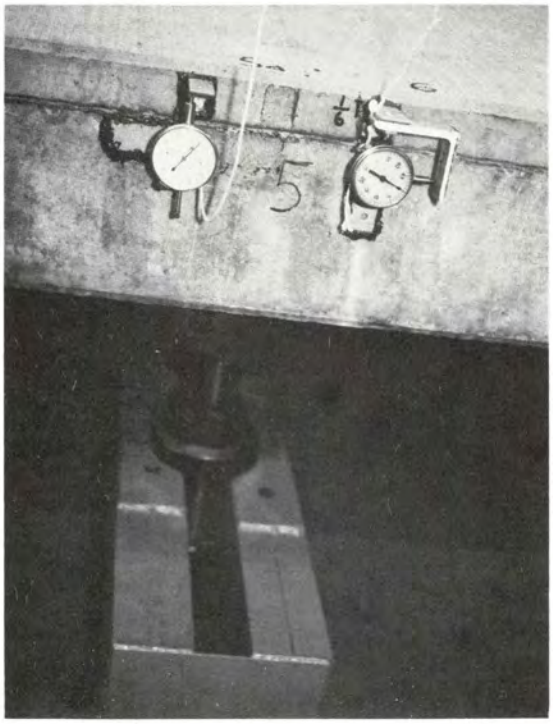

Fig. 3.6 Slip and Separation Dials on the Side

the second phase of testing three four-inch travel 0.001-inch, dial indicators were attached to the box frame above the slab (Fig. 3.11) to measure the midspan deflection. The deflectometers were removed in this part of the test.

Loads were applied by means of hydraulic rams and measured by pressure cells which were calibrated prior to testing.

3.3 TESTING PROCEDURE

Two series of tests were conducted on the model bridge span, (a) Load distribution tests, and (b) Ultimate load tests.

3.3.1 LOAD DISTRIBUTION TESTS

In order to establish the applicability of existing methods of predicting the lateral load distributions to the proposed bridge system a test was conducted. The loading for this test consisted of a single concentrated load applied at points on a uniformly spaced grid on the slab. The concentrated load used for this test had a magnitude small enough not to cause any cracking of the bridge and large enough to produce measurable deflection in all box members. A load level of 8.0 kips was applied by means of a 20 ton ram attached to a movable frame above the slab. A total of 30 load points as indicated in Fig. 3.7 were used. The applied load was distributed over an area of 8" by 8" as shown in Fig. 3.8. With the application of 8.0 kips load at each load point, deflectometers and strain meters were read.

3.3.2 ULTIMATE LOAD TEST

Since it has been reasonably well established that the lateral

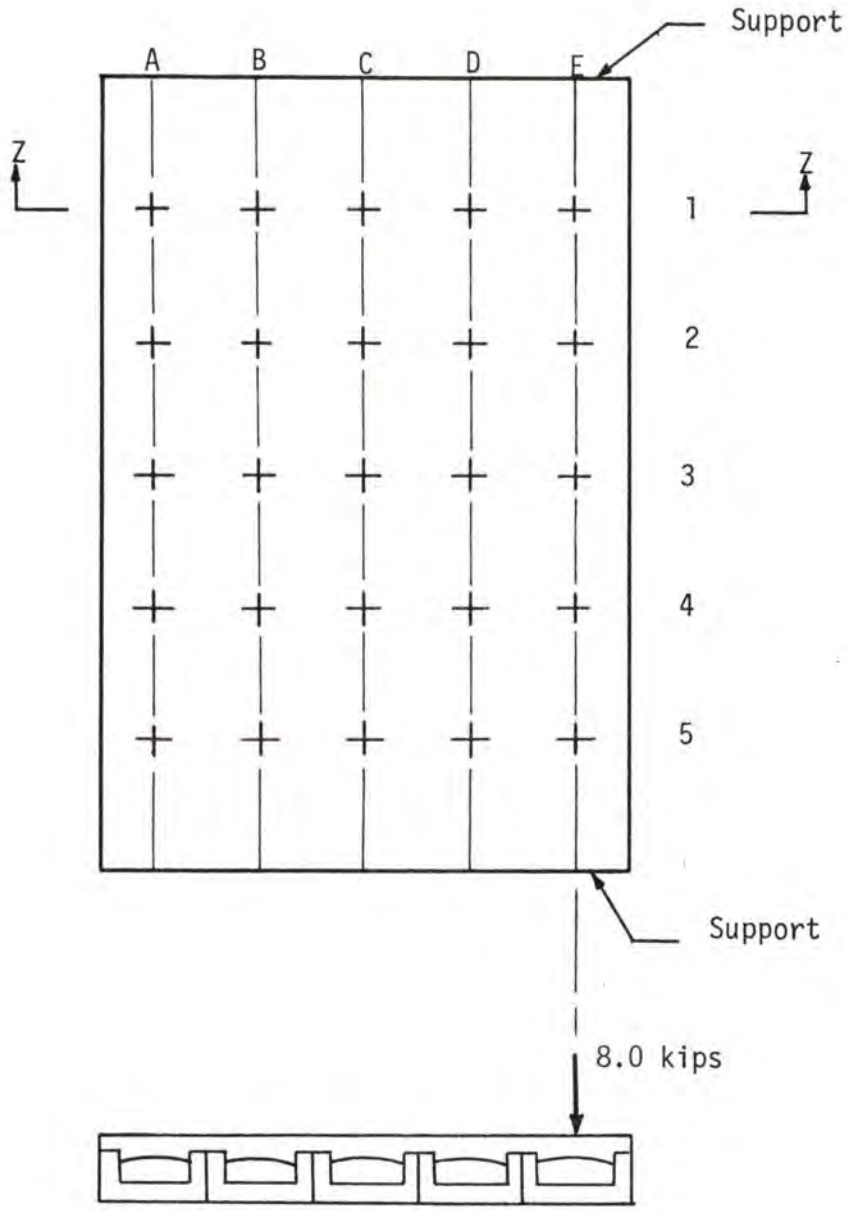

Section Z-Z, Load at E-1

Fig. 3.7 Locations of Loading Points For Load Distribution Test

distribution of loads in a bridge span are consistent up through normal overload ranges[9], the ultimate load test was designed to test the composite action of the proposed system. For this purpose a simulated highway truck loading was considered.

A maximum moment condition for H20-S16 truck load when applied to the full scale bridge is shown in Fig. 3.9(a). As indicated in the figure the front wheel load is only 8" from the support point. This distance will reduce to 4" for the model slab and for testing purposes would mean loading directly over the support. Also, maintaining a load differential between the front wheel load and the rear wheel load would be particularly difficult. Therefore, a two point loading system considering only the trailer wheel loads was adopted, Fig. 3.9(b). In addition, to provide a constant moment region for instrumentation, wheel loads were applied symmetrically at one-third points of the span, Fig. 3.9(c).

The model trailer was assumed to be 6' long and 3'-4" wide and represented by four loading points. The dual tire impression as estimated by the Pickett & Ray method[16] was used to simulate the tires, Fig. 3.10.

Tension rods secured in the laboratory floor and extending through holes drilled in the slab were used as the loading axis. The tension rod also extended through 30 ton rams which were used to transfer the applied load to the slab, as shown in Fig. 3.10 and 3.11.

The simulated trailer loading was alternated in four different arrangements, in order to consider the most common positions of the trailer over the slab and to determine the most adverse condition for

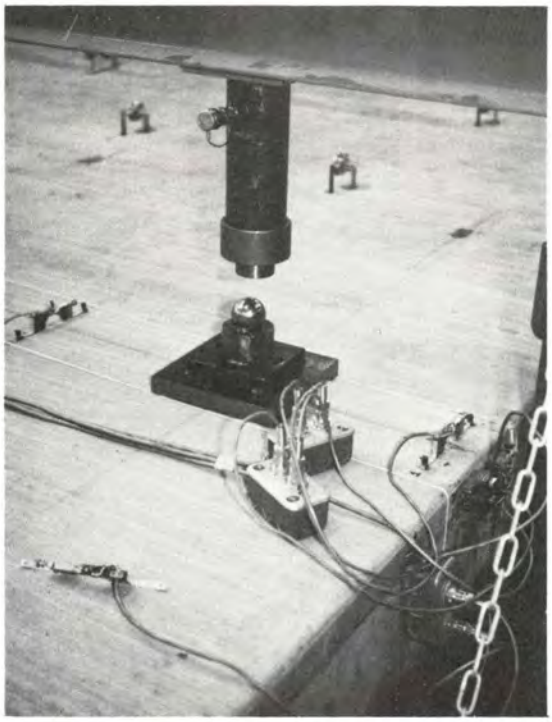

Fig. 3.8 Load Distribution Test in Progress

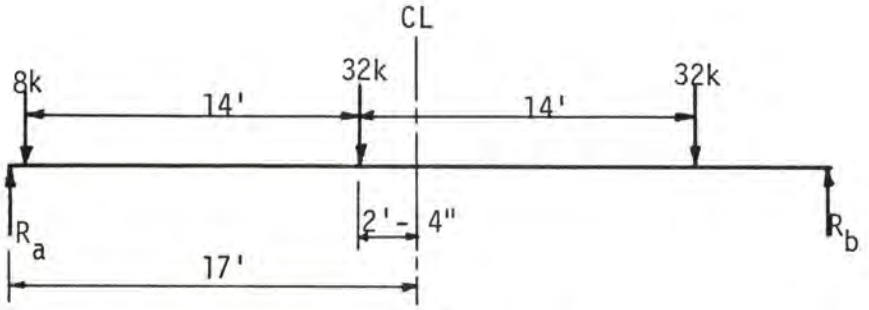

$M_{max.}$ = 343.5 k-ft

(a) H20-S16 Load on Full-Scale Bridge

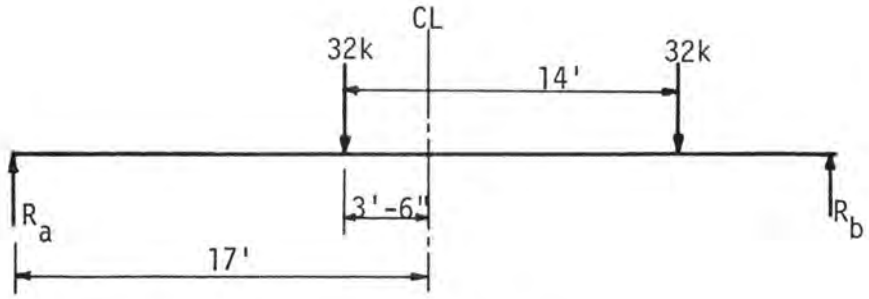

$M_{max.}$ = 332 k-ft

(b) S16 Trailer Load on Full-Scale Bridge

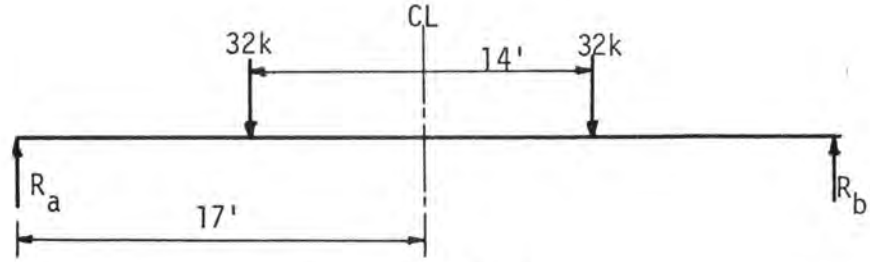

$M_{max.}$ = 320 k-ft

(c) Full-Scale Loading Comparable to the Model Test

Fig. 3.9 Truck Loading For Maximum Moment

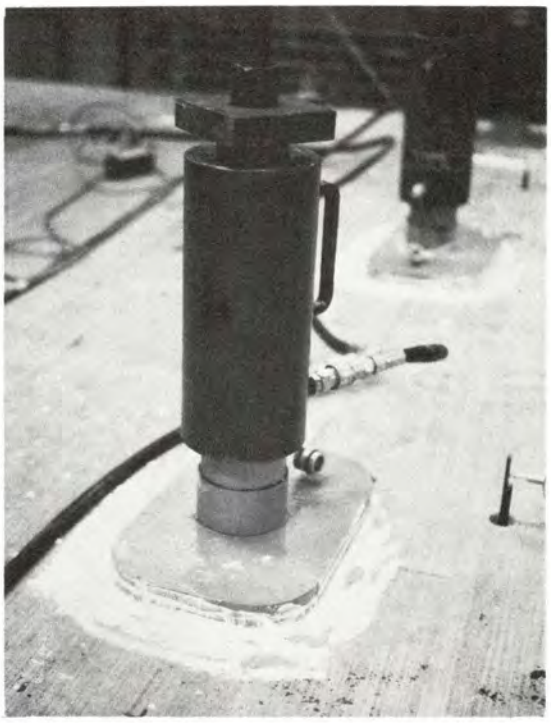

Fig. 3.10 Simulated Dual Tire for S16 Trailer

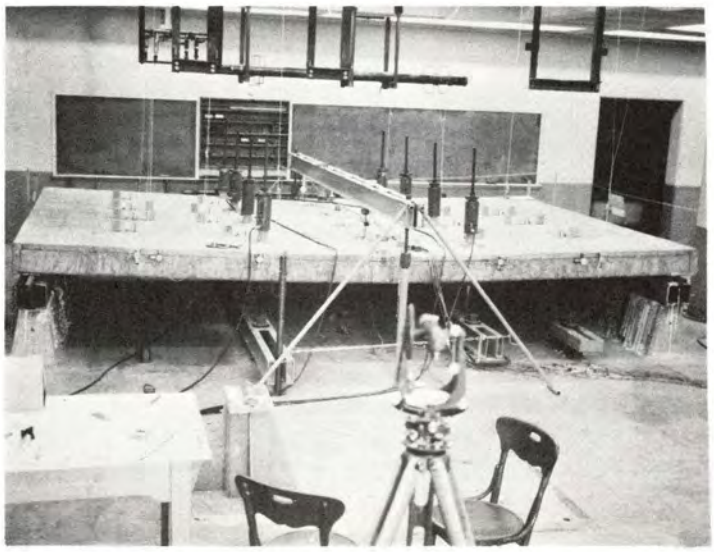

Fig. 3.11 Trailer Loading Test in Progress

slab failure. Fig. 3.12 shows the four alternating loading arrangement.

Loads were applied at increments of 4.0 kips at lower loads and at high overloads an increment of 1.0 kip was adopted. At every load level all the instruments were read and crack patterns were observed. The system was then completely unloaded in order to reload the slab for a different trailer position and to observe permanent displacement.

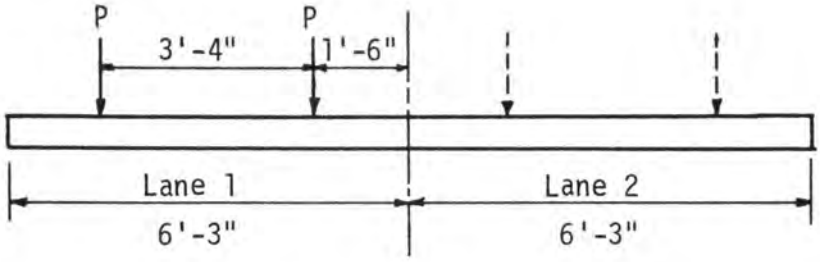

(a) Trailer in Lane 1 or Lane 2

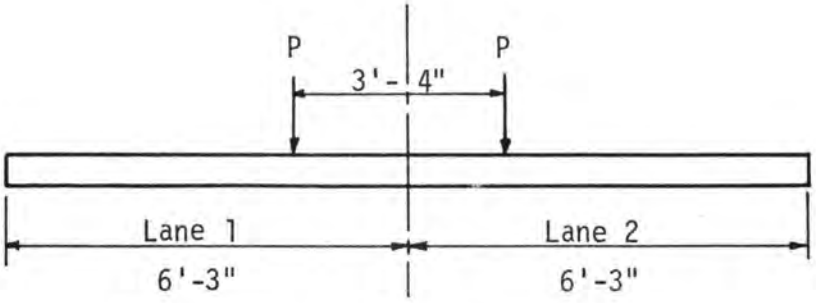

(b) Trailer at the Center of Roadway

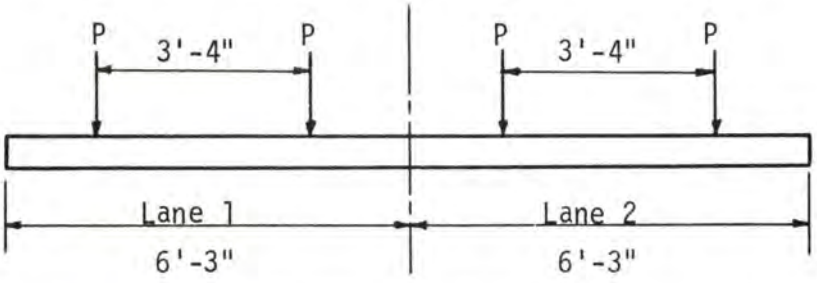

(c) Trailers on Both Lanes

Fig. 3.12 Alternate Loading Arrangement for Simulated Trailer Test

CHAPTER IV

RESULTS AND DISCUSSIONS

4.1 GENERAL

Results of the tests performed on the model bridge slab are presented in this chapter. Load distribution test data were used to generate influence surfaces of deflection for various load location, and were compared with the theoretical load distribution behavior as predicted by the Guyon-Massonnett theory.

Experimental results of the ultimate load test series were also utilized to obtain the load distribution factors which may be applied in designing this particular type of member for AASHO loading, both in service load level and high over-load conditions. Finally, a discussion of the ultimate capacity and the mode of failure of the test bridge slab is presented.

4.2 EXPERIMENTAL RESULTS

4.2.1 Load Distribution Test Data. During this series of tests, readings from five deflectometers installed at mid span beneath each box unit were recorded for each position of the load. Thus by repeating this procedure for all the thirty load locations and utilizing Maxwell's reciprocal theorem, it was possible to obtain the deflection of the model at thirty points on the slab caused by an 8.0 kips load applied to each box unit at midspan. Since the applied load was well within the elastic range, unit load deflections were obtained by simply dividing the deflection data by the 8 kip load. Figures 4.1, 4.2 and 4.3 are the influence surfaces for deflection when the unit load is applied at exterior, interior, and middle units respectively. The displacement values are shown

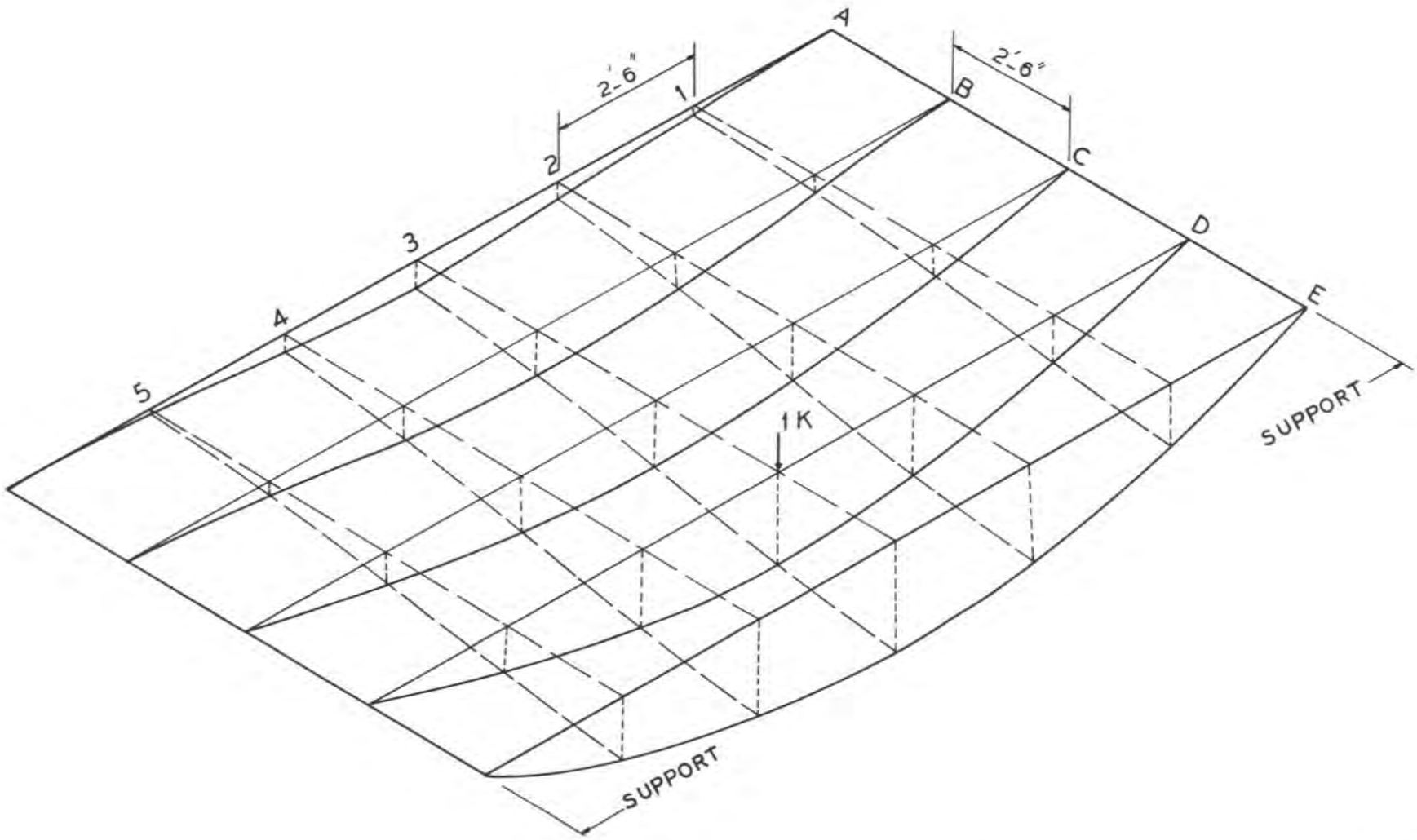

Fig. 4.1 Influence Surface for Deflection - Load at E-3

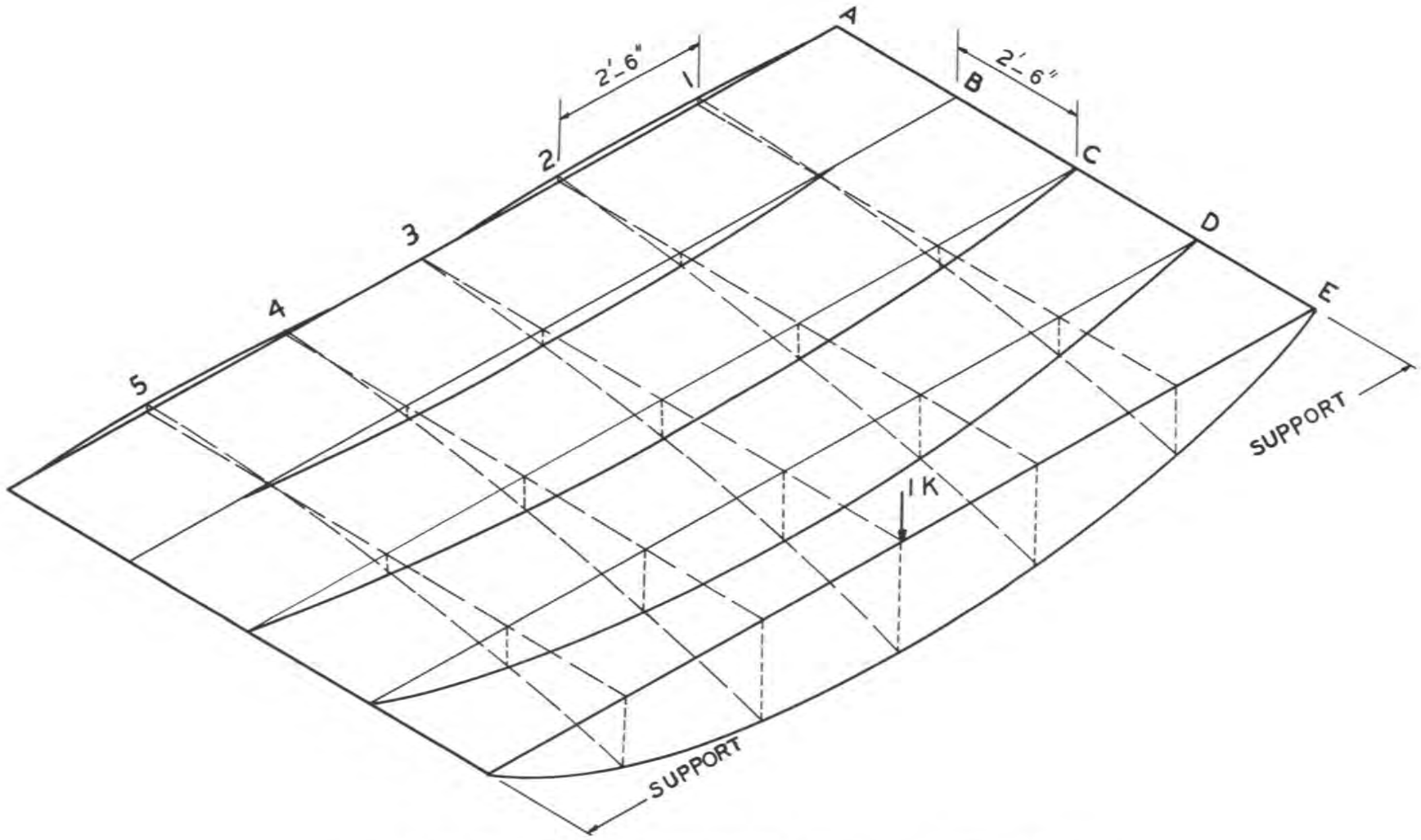

Fig. 4.2 Influence Surface for Deflection - Load at D-3

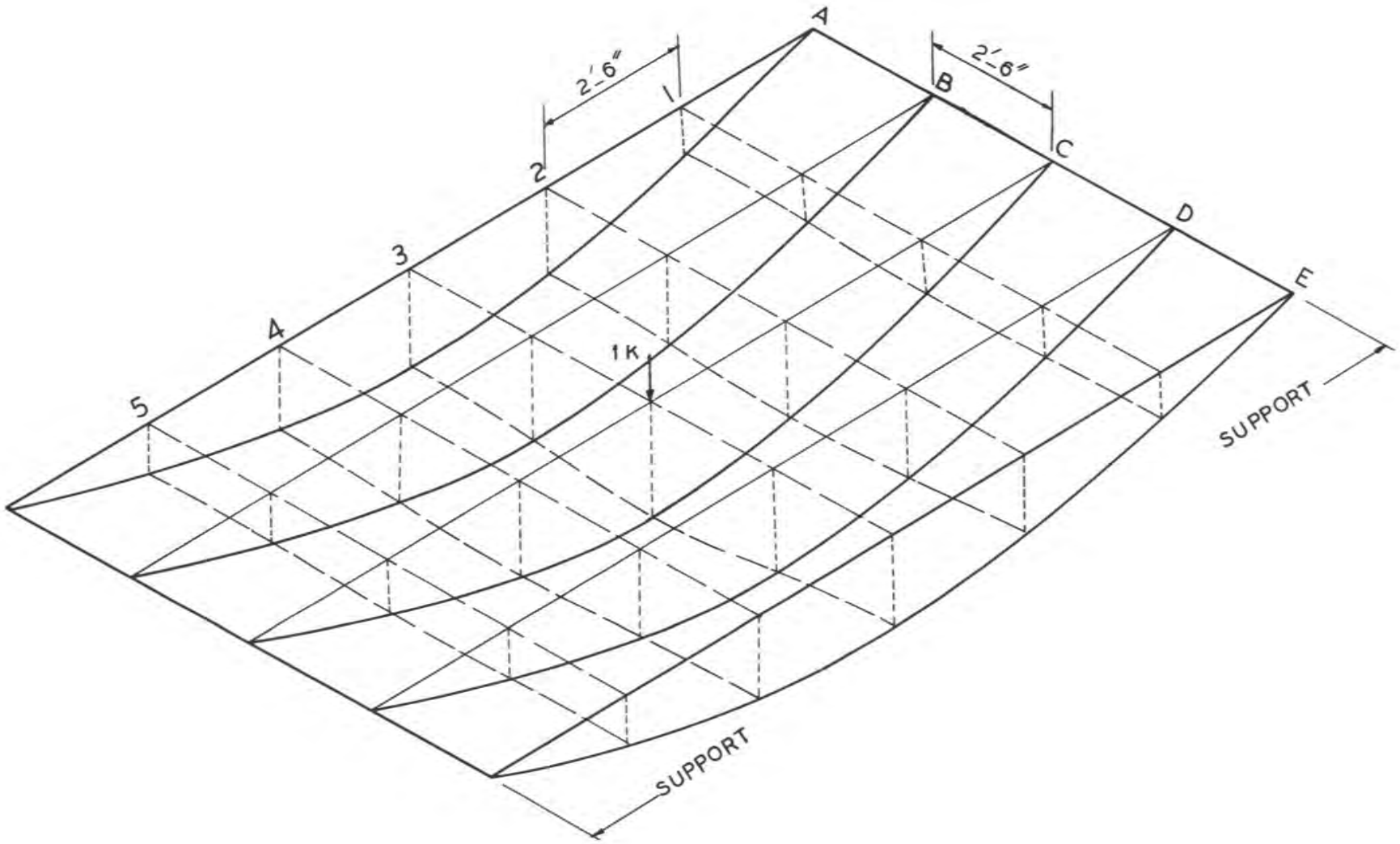

Fig. 4.3 Influence Surface for Deflection - C-3

LOAD AT E - 3

	A	B	C	D	E
1	-0.38	0.10	0.73	1.65	2.93 *
2	-0.16	0.51	1.51	2.65	4.05
3	0.00	0.76	1.69	2.93	4.65
4	-0.16	0.54	1.51	2.57	4.19
5	-0.42	0.12	0.76	1.71	2.95

LOAD AT D - 3

	A	B	C	D	E
1	0.16	0.38	0.77	1.13	1.43
2	0.25	0.86	1.54	1.99	2.47
3	0.43	1.09	1.74	2.36	2.95
4	0.38	0.91	1.56	2.06	2.49
5	0.11	0.36	0.79	1.20	1.61

LOAD AT C - 3

	A	B	C	D	E
1	0.78	0.82	0.96	0.91	0.86
2	1.55	1.60	1.74	1.60	1.42
3	1.83	1.97	2.01	1.83	1.65
4	1.52	1.60	1.78	1.60	1.51
5	0.86	0.89	0.91	0.89	0.86

*All values are in inches x 10^{-3}

Table 4.1 Grid Point Deflections Due to Unit Load

in table 4.1. Due to symmetry, when the load was applied at either of exterior and interior units, deflection readings from the symmetrical quadrants were averaged to produce figures 4.1 and 4.2

The load distribution characteristics of the model bridge slab were studied utilizing the lateral distribution of deflection under the action of the single load applied at the various grid locations. This was done by expressing the deflection of every box unit as a percentage of the sum of the deflections of all five units at the cross-section under consideration. In this way it has been possible to made a direct comparison of the deflection behavior of the bridge with that predicted by the Guyon-Massonnet theory for the lateral distribution of load. Moreover, the percentage of the sum of the deflections carried by every unit is a non-dimensional quantity which may physically represent the fraction of load or moment carried by each unit. This fact is easily verified in the elastic range since the deflections are linearly proportional to loads and moments. As shown in Chapter II, the theoretical procedure does not involve any deflection computations and represents any physical behavior of the system in a general sense. Figures 4.4, 4,5, and 4.6, which represent the cross-sections of the bridge when an 8.0 kip load is applied at the center of various units, were obtained by this method. Since test data were taken for all the 30 load points, as shown in Fig. 3.7, a weighted average of the data at various cross-sections was used to increase the accuracy of the data by increasing the number of usable data points at each loading. More weight was given to data taken at midspan since the cross-section close to support showed less

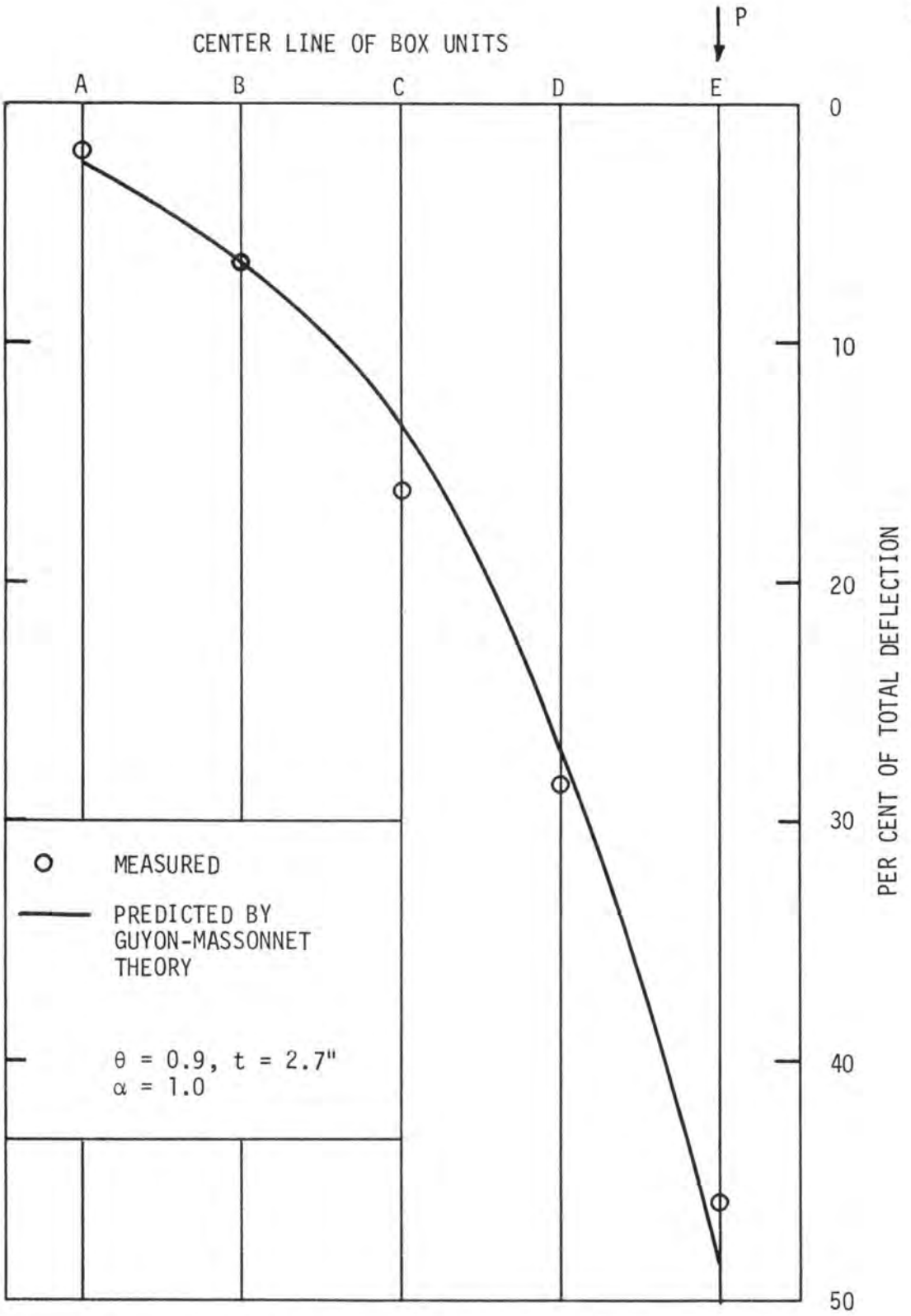

Fig. 4.4 Deflection Distribution - Load on E

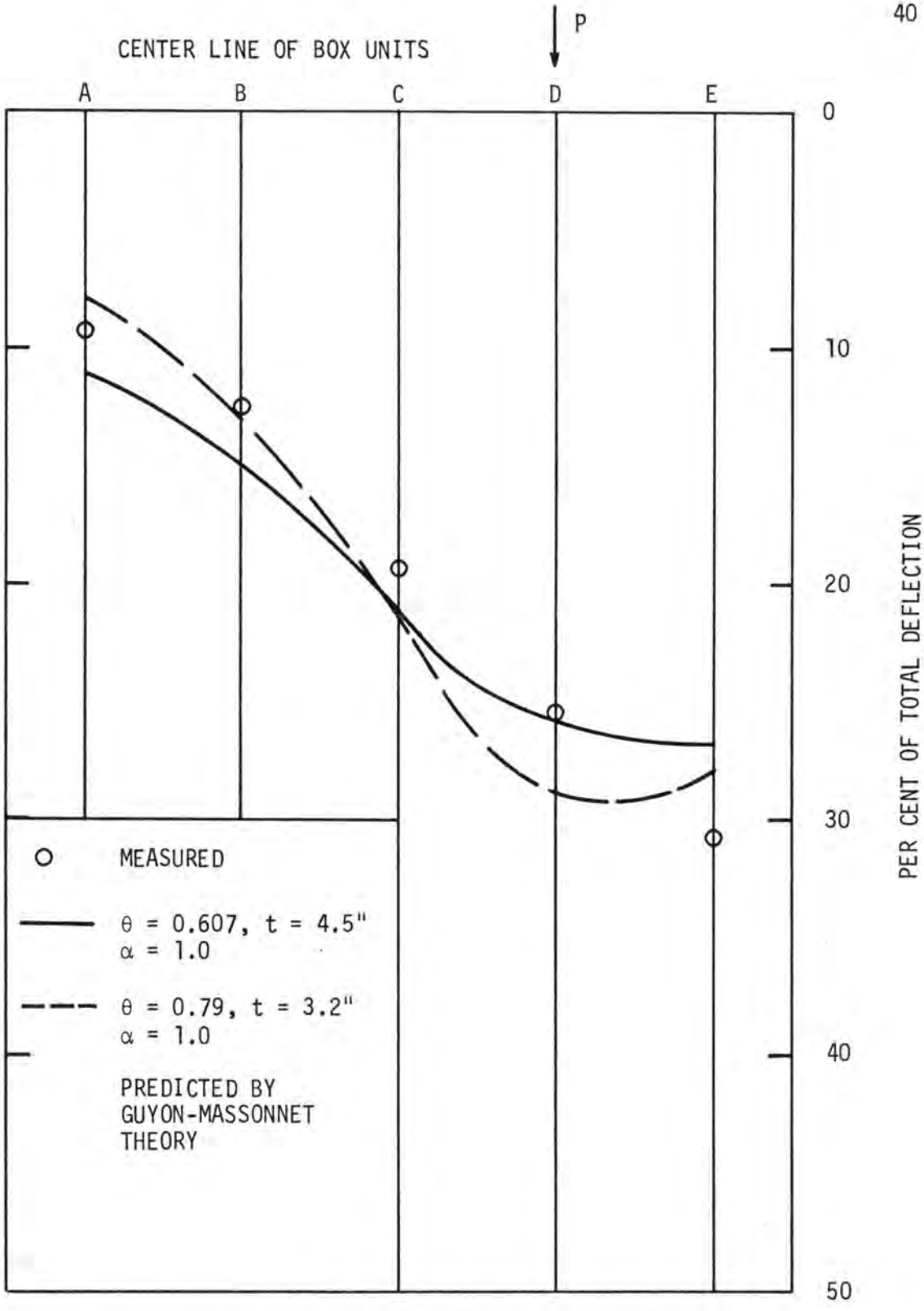

Fig. 4.5 Deflection Distribution - Load on D

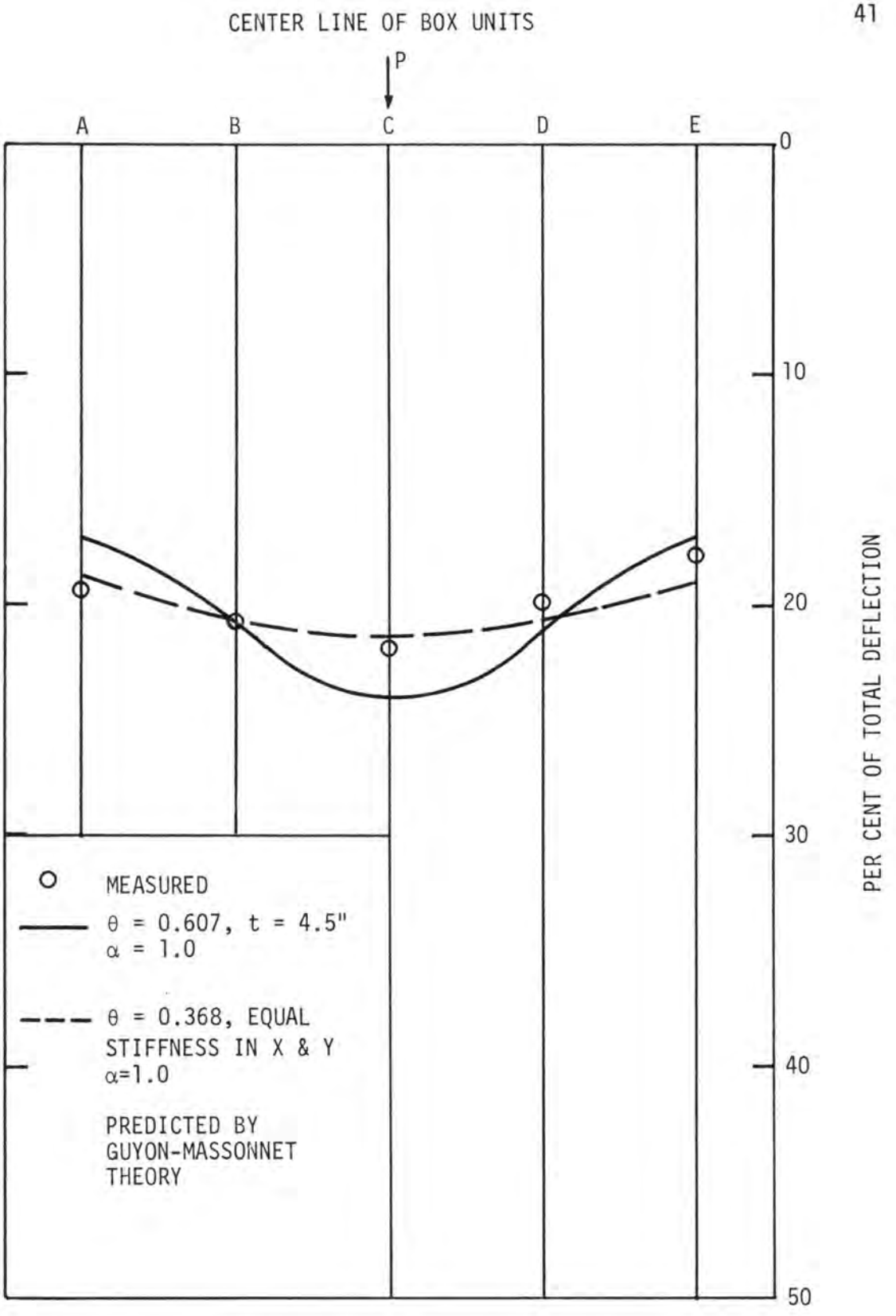

Fig. 4.6 Deflection Distribution - Load on C

distribution characteristics due to the edge conditions.

4.2.2 The Ultimate Loading Test Data. During this phase of testing, a simulated S16 trailer load was applied at alternate positions on the bridge slab. The trailer position was alternated at a number of load levels to determine the controlling condition of loading. From the distribution behavior of the bridge in the first test series it was determined that the most critical condition of loading for composite action is when both lanes are loaded simultaneously. Therefore, at high loads close to failure, loading was not alternated and was applied to both lanes.

At every load level all instruments were read and recorded. Slip and slab separation dials did not show any significant quantity. The maximum slip and separation recorded prior to failure were .015" and .0009", respectively. Included in these readings was a curvature effect of the slab, which at high load and large curvatures makes the readings less significant. The flexural failure and ultimate deflection of the bridge also confirmed the insignificance of the measured slip and separation values.

Strains were measured at midspan on the top and bottom of each section and on the outside of the exterior members. Strain profiles along the depth of the bridge slab are shown in Fig. 4.7. Composite behavior of the bridge slab up to the failure load was confirmed from this data.

Load-deflection data were obtained during the testing and are shown in Fig. 4.8. This figure also includes the last unloading cycle before failure. The predicted load-deflection curve was obtained through

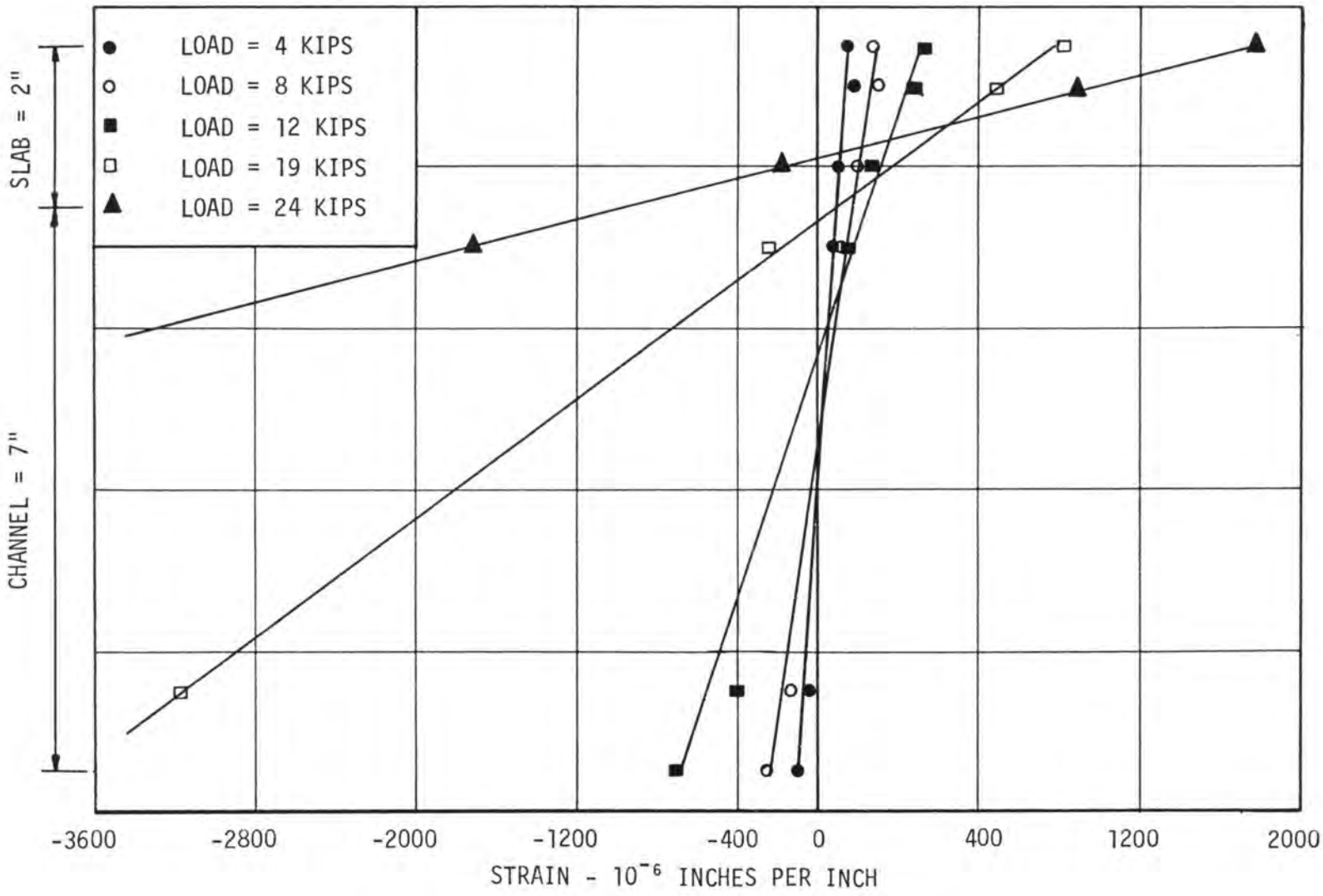

Fig. 4.7 Strain Distribution in Exterior Unit

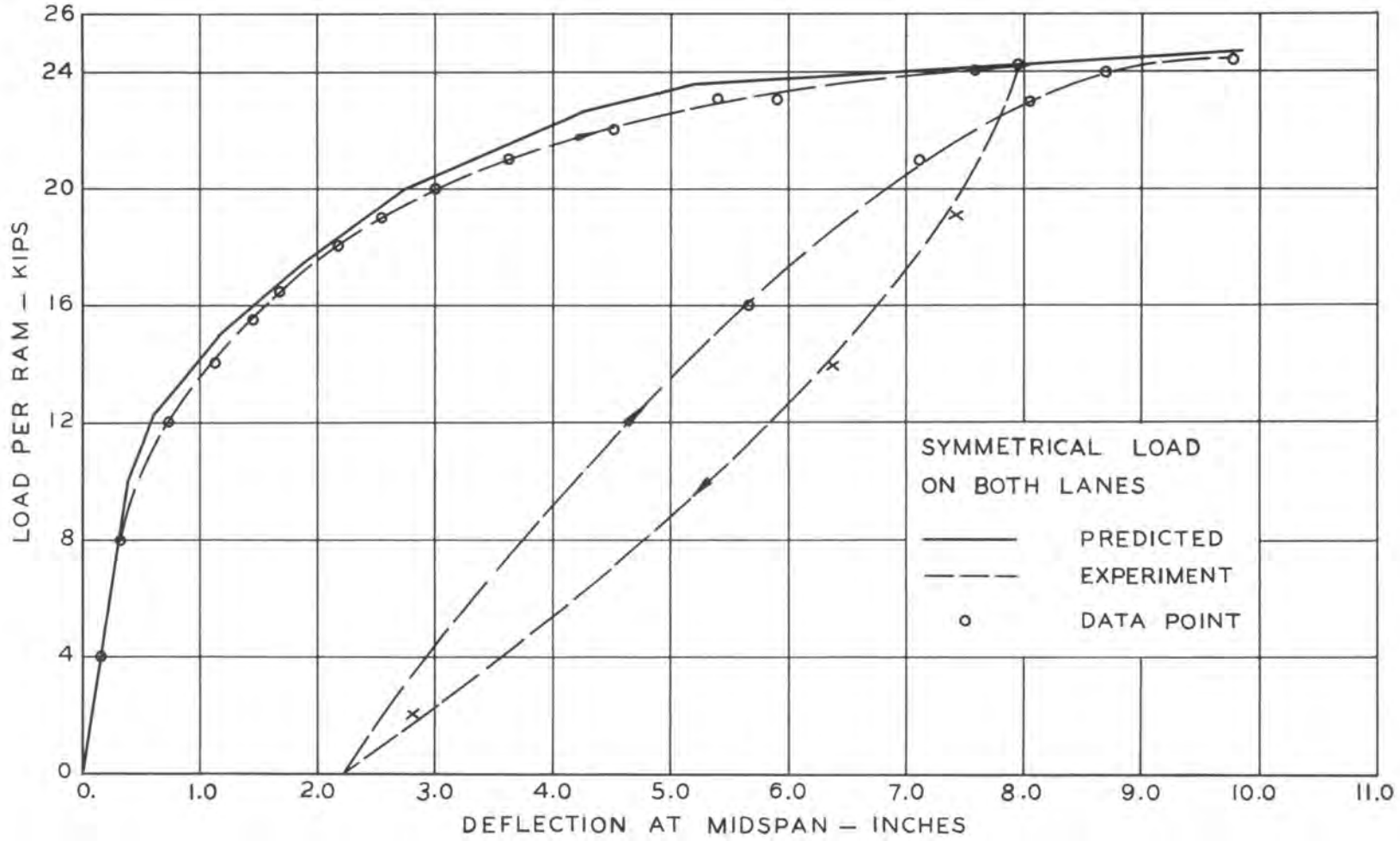

Fig. 4.8 Ultimate Test - Load vs. Deflection

an interative procedure[1] for the case of complete composite action of the bridge slab. It should be noted that Fig. 4.8 corresponds to the case when both lanes are loaded simultaneously. The deflection data obtained during the alternate trailer position were utilized to evaluate the wheel load distribution coefficients which were compared to those given by AASHO specifications and will be discussed later.

4.3 COMPARISON BETWEEN THEORETICAL AND EXPERIMENTAL RESULTS

4.3.1 Load Distribution Behavior. The influence surfaces for deflection, as presented in Figs. 4.1, 4.2 and 4.3, indicated that the model bridge slab behaved elastically. The deflections listed in the accompanied table showed that almost identical values were obtained for cross sections symmetrical with respect to the loaded section. This further indicates a behavior similar to that of an orthotropic elastic plate which justifies the application of the Guyon-Massonnet distribution theory.

A comparison of the above mentioned theory with the experimental deflection data was made in Figs. 4.4, 4.5, and 4.6. As stated previously, the theoretical distribution pattern is a function of two parameters; the flexural stiffness parameter θ, and the torsional stiffness parameter α. In order to evaluate θ and α it was necessary to compute the flexural and torsional stiffnesses of the members in the longitudinal and transverse directions. Longitudinal stiffnesses were computed by assuming a simplified rectangular box section, however it was not possible to clearly define the transverse stiffness of the model bridge slab.

Considering Fig. A.1 in the appendix, it can be seen that at various section normal to the y-axis the transverse stiffnesses will vary considerably. Therefore it would be inaccurate to assume uniform stiffness in the y-direction. It is also noted that the weakest section is at the joint of two channels where only the top slab with a thickness of 2" contributes to transverse stiffness. At any section within the box unit, not only the top slab is thicker but also the prestressed channel itself contributes to flexural and torsional stiffnesses.

A further complication arises from the fact that for the weakest section (joint of channels) stiffness properties change with the intensity and position of load. Since the legs of two adjacent channels could bear against each other either at the top or at the bottom depending on the direction of curvature of the slab, this would obviously increase the stiffness at the joint of the units.

Therefore, for the purpose of this comparison several effective thicknesses of the top slab were assumed and the Guyon-Massonnet distribution prediction was carried out for each case as shown in the appendix. For every load position a number of predicted curves were compared to experimental data to find the one which physically corresponds to the data. In Fig. 4.4, where the load was applied to exterior unit E, prediction corresponding to t = 2.7" (thickness of top slab) best fits the test data. It can be seen that when the load is on E, the contact of the channel legs at the top does not contribute much to transverse stiffness. The bottom of the channels which could contribute to the transverse stiffness unfortunately were not bearing on each other. The thickness of 2.7" corresponds to an equivalent top slab with uniform

thickness and is approximately equal to the thickness of the slab over the channel legs plus the depth of the high strength grout placed between the channel at the top to prevent concrete leakage during casting of the top slab.

In Fig. 4.5 two cases were considered. The solid line curve corresponds to the maximum thickness of the top slab, 4.5", and the dashed line corresponds to t = 3.2", an average of t = 4.5" and t = 2.7". It can be seen that in the vicinity of the load the distribution corresponding to t = 4.5" best agrees with the test data. While away from the load, t = 3.2" gives better agreement with test data. It can also be noted that the exterior units, A and E, deviate even from the dashed line since one side of these units is free from effect of adjacent members.

As shown in Fig. 4.6, data points correspond to very high transverse stiffness which indicates very good load distribution behavior. The dashed curve corresponding to the case of equal flexural stiffness in both directions fits the data point very closely. However, equal stiffnesses in x and y direction physically correspond to a monolithic box girder slab which is unrealistic and cannot be justified. On the other hand, the geometry of the slab, the length width ratio, and the boundary conditions would help to produce the effect observed in the test data.

In general, it can be seen that the Guyon-Massonnet theory, which originally was developed for I-girder composite slabs, can predict distribution behavior of this particular system provided special consideration is given to the interaction of the adjacent units.

4.3.2 Wheel Load Distribution Behavior. Since the results of the load distribution test were found to be in reasonable agreement with

the Guyon-Massonnet theory, the simulated truck loading data were utilized to obtain the wheel load distribution patterns of the model slab for various positions of the trailer. In Fig. 4.9 the model trailer with 4.0 kips on each wheel simulates the S16 trailer loading. The trailer position is approximately at the critical position of load for exterior unit E when only one lane is loaded. Test data indicates that Unit E carries 0.682 of one wheel load. AASHO specification, section 1.3.1.B gives the wheel load distribution for exterior girder as $\frac{We}{7.0}$ in the case of monolethic concrete box girders. "We" is the width of the exterior girder measured from the midpoint between girders to the outside edge of the slab. Considering the full scale bridge, We = 5.0' for this particular system since there was no slab overhang. Thus, experimentally the ratio is $\frac{We}{7.32}$, which indicates distribution behavior superior to that required by the AASHO specifications for concrete box girders. The same concept is applied in Fig. 4.10 where a high overload of 20 kips was applied. Due to excessive cracking of the channels, theoretical predictions were based on equal stiffness in x and y directions. In this case the load distribution is more uniform and unit E carries only 0.54 of one magnified wheel load of 20 kips. Again, this results in $\frac{We}{9.25}$ which is again superior to the AASHO requirements for concrete box girders design.

Since the loading system was rigidly fixed to the testing floor, it was not possible to load both lanes unsymmetrically to obtain the most critical position of two trailers for overload distribution characteristics. However, the symmetrical loading, as shown in Fig. 4.11, approximately represents the critical condition for all the units when considering composite behavior. In this case the experimental

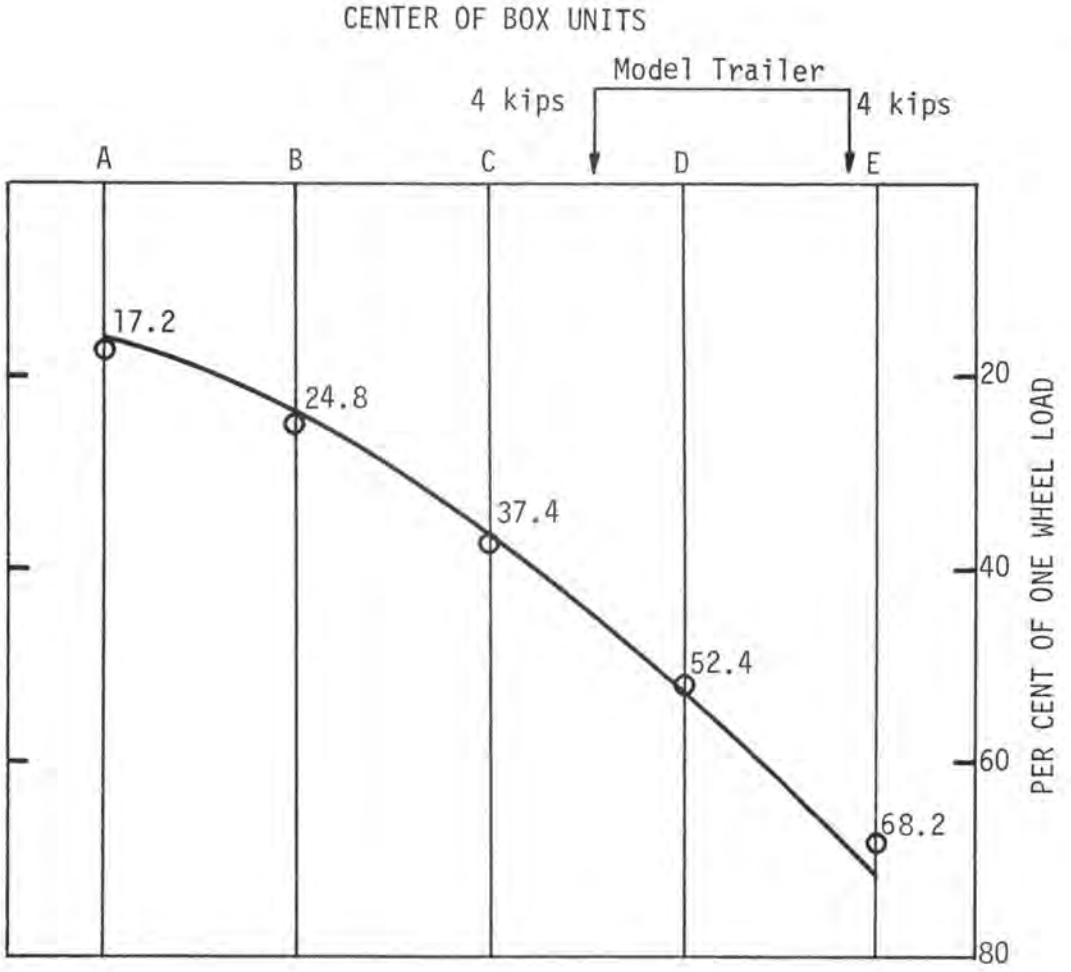

O MEASURED

——— COMBINATION OF $\theta = 0.9$ AND $\theta = 0.607$
$\alpha = 1.0$ (See Figs. 4.4, 4.5)

MAXIMUM LOAD ON UNIT E

FRACTION OF WHEEL LOAD:

AASHO - CONCRETE BOX GIRDERS $\frac{We}{7.0} = 0.715$

EXPERIMENTAL $\frac{We}{7.32} = 0.682$

Fig. 4.9 Wheel Load Distribution of S16
Model Trailer on One Lane

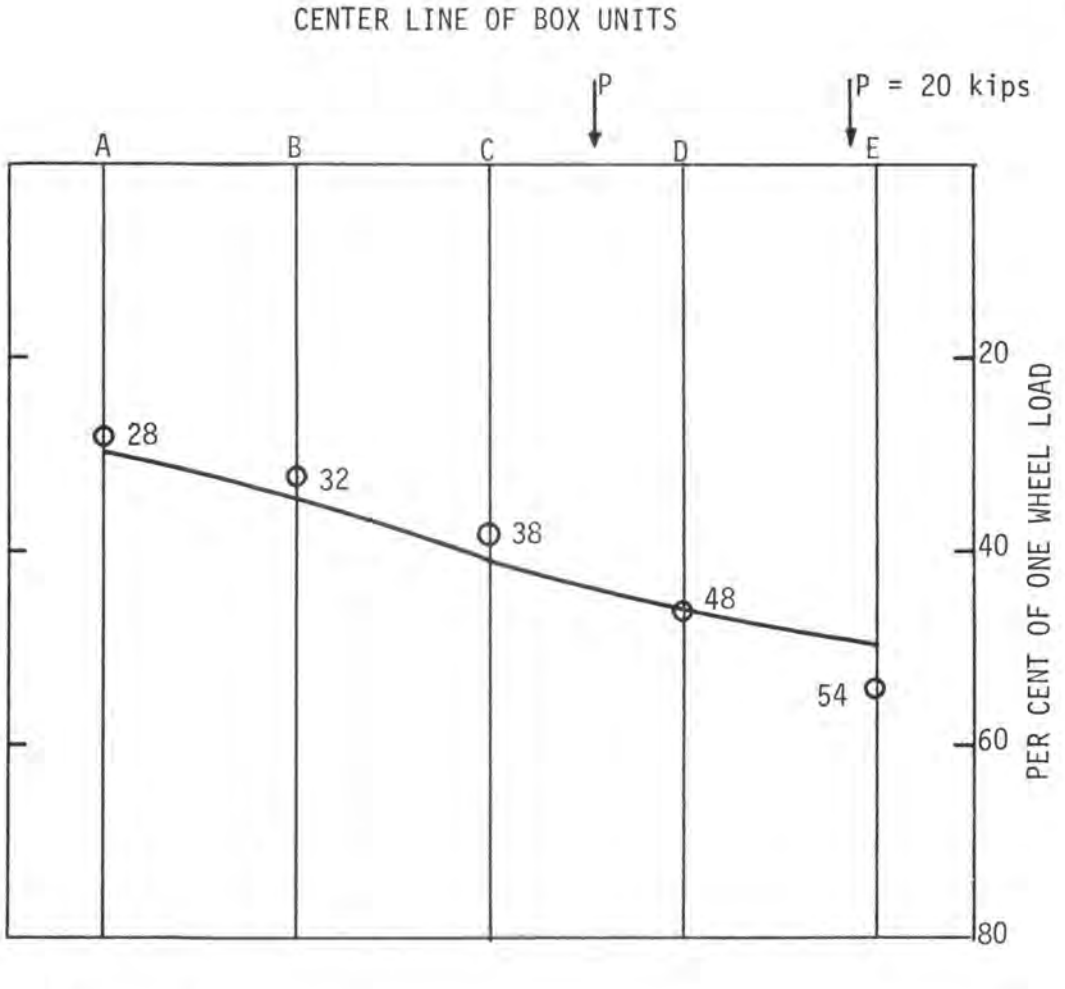

O MEASURED

—— θ = 0.368 EQUAL STIFFNESS IN X & Y
α = 1.0 (See Discussion on page 48)

MAXIMUM LOAD ON UNIT E

FRACTION OF WHEEL LOAD:

AASHO CONCRETE BOX GIRDERS $\frac{We}{7.0} = 0.715$

EXPERIMENTAL $\frac{We}{9.25} = 0.54$

Fig. 4.10 Wheel Load Distribution at High Overload and Excessive Cracking

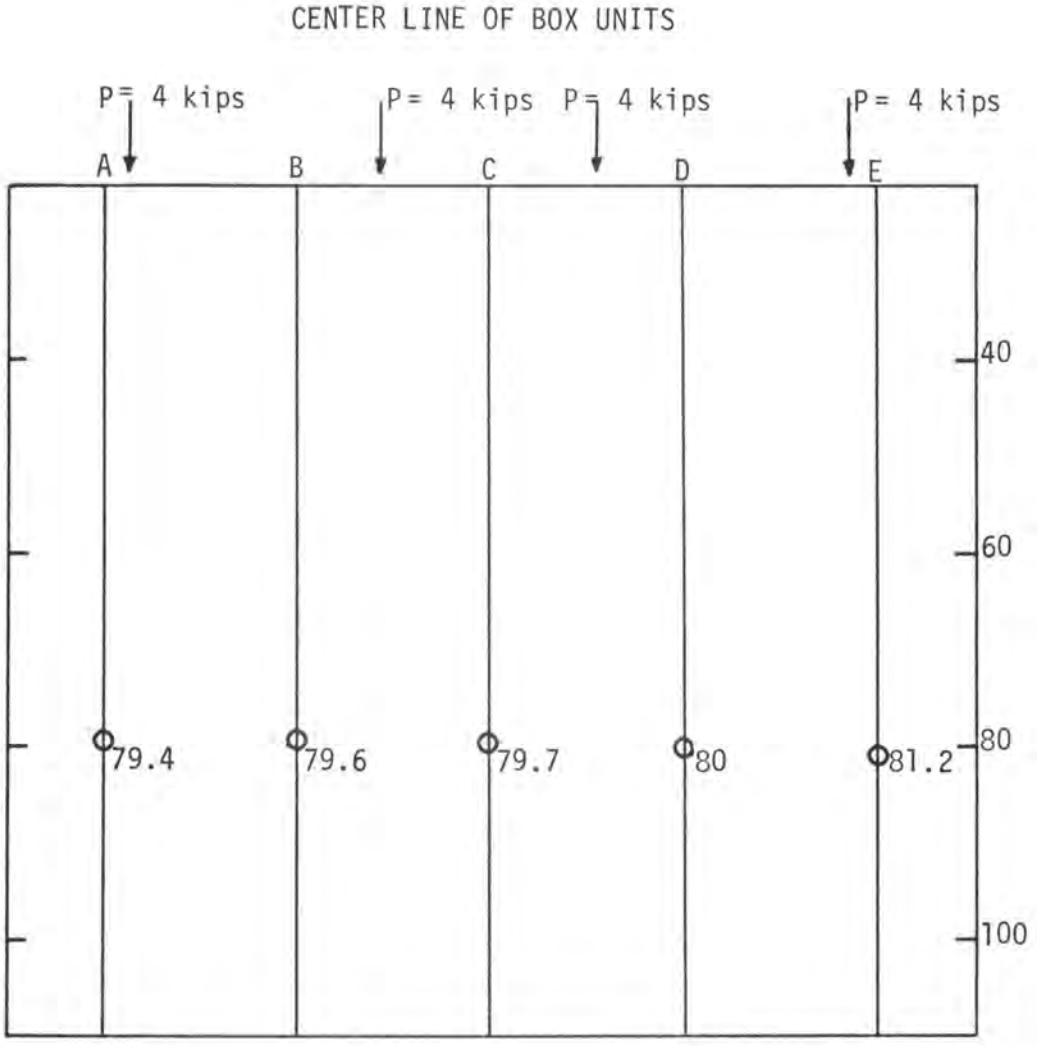

○ MEASURED

FRACTION OF WHEEL LOAD:

AASHO CONCRETE BOX GIRDERS
CONSIDERING TOTAL CROSS SECTION = 0.8 = $\frac{We}{6.25}$

EXPERIMENTAL (MAXIMUM) = 0.812 = $\frac{We}{6.15}$

Fig. 4.11 Wheel Load Distribution When Both Lanes Loaded

wheel load distribution is much higher than the previous cases which justifies the earlier assumption in this chapter that the critical condition of loading is when both lanes are loaded simultaneously. It is noted that $\frac{We}{6.15}$, found experimentally, is larger than the AASHO ratio, which is the most logical result since the proposed system can at best behave as a monolithic box girder system. For this condition the AASHO specifications require that the total cross section of the bridge be designed to accomodate the total live load and dead load in each span. For the case considered in the study the minimum distribution factor for both lanes loaded was 0.8 which corresponds to $\frac{We}{6.25}$.

4.3.3 Ultimate Behavior and Mode of Failure. Since failure was expected to occur when both lanes were loaded, in the later stages of the test all eight rams were loaded simultaneously with small increments of load. Load-deflection data is shown in Fig. 4.8. At 24.0 kips per ram the bridge slab was unloaded and a permanent deflection of 2.25" was observed. Then the specimen was reloaded until failure occurred at 24.5 kips per ram or 19.6 kips per unit. Measured deflection just before failure was 9.75". These quantities were very close to those predicted for the failure condition. Based on conventional ultimate strength design, and the assumption of complete composite action, failure load was estimated as 24.7 kips per ram or 19.75 kips per unit, and the corresponding deflection was calculated as 9.826".

Therefore, the agreement between predicted and the actual failure load confirms the complete composite flexural failure of the slab as shown in Fig. 4.12 and 4.13. Prior to failure load some cracks appeared on the top of the slab in the longitudinal direction. These cracks

Fig. 4.12 Failure as Viewed from the Side

Fig. 4.13 Compression Failure at the Top Slab
as Viewed from the Top

started from the support and gave the expectation that the top slab might fail in the longitudinal direction. However, at the failure load a large crack was developed at the vicinity of the loaded section in the transverse direction which caused the sudden compression failure of the top slab as shown in Fig. 4.13.

CHAPTER V

SUMMARY AND CONCLUSIONS

5.1 SUMMARY

A one-half-scale concrete composite model bridge slab was studied to evaluate the structural performance of a 36-foot long, two-lane, highway bridge span. A theoretical analysis of load distribution behavior based on the Guyon-Massonnet distribution theory is presented. Application of the theory to this particular bridge system is presented in an appendix together with a sample calculation.

An 18-foot long, 12'6" wide model bridge composed of five prestressed channel and a cast-in-place top slab was constructed for the purpose of experimental evaluation. The model bridge was tested as simply supported on two opposite edges only. The specimen was instrumented to measure strains, deflection, and slip and slab separation at the interface of the two composite components.

Two series of tests were conducted in this study. In the first series of tests a single concentrated load was applied to a grid of 30 load points. Deflection was measured at midspan beneath every box unit and utilizing the Maxwell's reciprocal theorem it was possible to construct influence surface of deflection and to study the distribution pattern of load. The load distribution behavior was studied in non-dimensional deflection percentages. The share of deflection, load, or moment carried by each unit was expressed as a percentage of the sum of the deflection of the five units.

In the second series of tests a simulated S16 trailer load was

applied to the two-lane model bridge slab. Wheel load distribution was studied, as in the first series of tests, and values were compared with those recommended by 1961 AASHO specifications. The ultimate behavior of the system and the failure mode were investigated. Complete composite action was observed throughout the test and the failure resulted from compression crushing of the top slab inside the constant live load moment region and in the vicinity of the load line.

5.2 CONCLUSIONS

Based on the results of this study, the following conclusions may be drawn:

1. The behavior of this type of bridge is essentially elastic when subjected to point loads, service wheel load, and even to appreciable overloads.

2. The transverse distribution of loads for this type of bridge structure at, and even above, service load level can be predicted reasonably well by the Guyon-Massonnet theory for load distribution, provided particular consideration is given to the transverse stiffnesses of this type construction. Special considerations arise from the fact that adjacent units transfer some load through the contact joint between channel sides.

This effective stiffness depends on the load position and must be considered in evaluating the actual stiffness in the transverse direction.

3. In the first series of the test, the exterior unit carried only 46% of the single concentrated load when applied directly at the center of this unit. Comparable tests on an I-girder precast-prestressed

concrete bridge, carried out at the Portland Cement Association, has shown that the exterior I-girder carried 67% of the load.

4. The wheel load distribution of this type of bridge was found to be comparable to monolithic concrete box girders as given by AASHO, 1961, which can be used for design of the proposed system.

5. The ultimate behavior of the model bridge slab was very satisfactory since complete composite action was observed up to failure. The failure load was closely predicted and was approximately six times the service load of S16 trailer.

6. The overall structural response of the half-scale model bridge slab was found to be satisfactory and in agreement with the predictions.

LIST OF REFERENCES

1. Salmons, J. R., and Poepsel, J. R., "Investigation of a Prestressed-Precast Composite Bridge System", Missouri Cooperative Highway Research Program Report 68-9, University of Missouri, Department of Civil Engineering, May 1968.

2. Salmons, J. R. and Mokhtari, S., "Model Study of a Prestressed-Precast Composite Bridge System", Missouri Cooperative Highway Research Program Report 68-9, University of Missouri, Department of Civil Engineering, June 1968.

3. Hetenyi, M., "A Method for Calculating Grillage Beams", S. Timoshenko 60th Anniversary Volume, New York, 1938, pp. 60-70.

4. Leonhardt, F., and Andra, W., " Die Veremfachte Tragerrost Berechnung", (The Calculation of Grillage Beams). Julius Hoffman Press, Stuttgart, 1950.

5. Morice, P.B., and Little, G., "Load Distribution in Prestressed Concrete Bridges Systems", The Structural Engineer, March 1954, Vol. 32, pp.83-111.

6. Rakshit, K.S., "Load Distribution in Bridge Decks: A Simplified Method", Indian Concrete Journal, July 1964, Vol. 38, March 1965, August 1965, Vol. 39.

7. Little, G., and Rowe, R. E., " Load Distribution in Multi-Webbed Bridge Structures from Tests on Plastic Models", Magazine of Concrete Research, Nov. 1955, pp. 133-142.

8. Wittrick, W. H., "Torsion of a Multi-Webbed Rectangular Tube", Aircraft Engineering, Vol. 25, Dec., 1953, p.372.

9. Mattock, A. H., Kaar, P. H., "Precast-Prestressed Concrete Bridges - Test of Half-Scale Highway Bridge Continuous Over Two Spans".

10. Johnston, S.B., and Mattoch, A.H., "Lateral Distribution of Load in Composite Box Girder Bridges", Highway Research Record, No. 167, 1967.

11. Goldberg, J. E., and Leve, H.L., "Theory of Prismatic Folded Plate Structures", International Association for Bridge and Structural Engineering Publications, Vol. 16, 1957, pp. 59-86.

12. Timoshenko, S., "Theory of Plates and Shells", McGraw Hill Co., 1959.

13. Rowe, R.E., "A Load Distribution Theory for Bridge Slabs Allowing for The Effect of Poisson's Ratio", Magazine of Concrete Research, July 1955, pp. 66-78.

14. Pickett and Ray, "Influence Charts for Concrete Pavements", Transactions, ASCE, 1951.

APPENDIX A

OUTLINE OF LOAD DISTRIBUTION CALCULATIONS FOR THE TEST BRIDGE

A.1 INTRODUCTION

In order to apply the Guyon-Massonnet load distribution theory to a particular bridge system the following basic quantities must be estimated.

(1) Width of the Equivalent Bridge As mentioned in Chapter II, the theory is based on the assumption that the actual grillage can be converted to an elastically equivalent system. The effective width of the equivalent bridge, to which the distribution coefficients K refer, depends upon the type of bridge under consideration. In the case of a slab bridge the equivalent bridge and the actual bridge are identical and the effective width is the same as the actual width. On the other hand, in the case of a bridge where the deck does not contribute to the strength of the girders, Guyon determined that the effective width exceeds the actual width by an amount equal to spacing of the girders. For a composite bridge where the deck slab acts with the girders and cantilevers beyond the outer girder a distance equal to half the girder spacing, the effective width is equal to the actual width. Thus:

b = effective width

b' = actual width

b_1 = girder spacing

then,

for a slab bridge $b = b'$

for an independent girder system $b = b' + b_1$

for a T-beam, I-girder or box girder composite bridge, b = b'

(2) The Effective Thickness of the Deck Slab. In most common cases, such as I-girder or T-beam bridges, the total deck slab contributes to the strength of the bridge and the effective thickness is therefore the actual thickness. However, for the case of the particular box bridge under consideration, the top slab thickness varies and the assumption of a uniform effective thickness is somewhat crude. Hence, several sets of distribution coefficients were computed for various effective thicknesses of the top slab and the set which best represented the particular loading case was used for comparison.

(3) The Torsional Stiffness of the Bridge. As mentioned in Chapter II, the Massonnet analysis has shown that the torsional stiffness of the deck slab which contributes to the torsional resistance of the bridge should in reality be taken as half the theoretical value. Also, the experimental works done at Cement and Concrete Association[7] have shown that for better agreement between theoretical and experimental distribution factors, torsional stiffness should be measured experimentally. The same investigaters have found Whittrick's formula for the torsional stiffness of a single box member to be accurate within 10 percent.

A.2 SAMPLE CALCULATION

Concrete Properties - as found from tests on 6" diameter cylinders:

Modulus of elasticity of the channels	4615 ksi
Modulus of rigidity $G = \frac{E}{2}$	2307 ksi
Modulus of elasticity of the top slab	4235 ksi
Modulus of rigidity $G = \frac{E}{2}$	2117 ksi
f'_c of prestressed channels	7810 psi

f'_c of the top slab 7245 psi

Composite Section Properties

Centroidal distance from bottom of member 4.53 in.

Moment of Inertia - transformed to f'_c of prestressed channel 1646.3 in^4

Equivalent box section with identical centroidal distance and moment of inertia is shown in Fig. A.1.

Flexural Stiffnesses

in the x-direction

$$\rho_x = \frac{E_c I_c}{b_1} = \frac{(4615)(1646.3)}{30} = 253.3 \times 10^3 \text{ Kip - in.}$$

in the y-direction

Assume thickness of top slab to be that of section B-B, Fig. A.1.

$t = 4.5"$

$I_s = 96.2\ in^4$, for a one-foot strip

$$\rho_y = \frac{E_s I_s}{L_1} = \frac{(4235)(96.2)}{12} = 33.9 \times 10^3 \text{ Kip - in.}$$

Flextural Stiffness Parameter

$$= \frac{b}{L} \sqrt[4]{\frac{\rho_x}{\rho_y}} = \frac{6.25}{17} \sqrt[4]{\frac{253.3}{33.9}}$$

$$= 0.607$$

Torsional Stiffnesses

in the x - direction: Whittrick's formula for a single box section

$$K = \frac{4A^2}{\oint \frac{ds}{t}}$$ (refer to Chapter II)

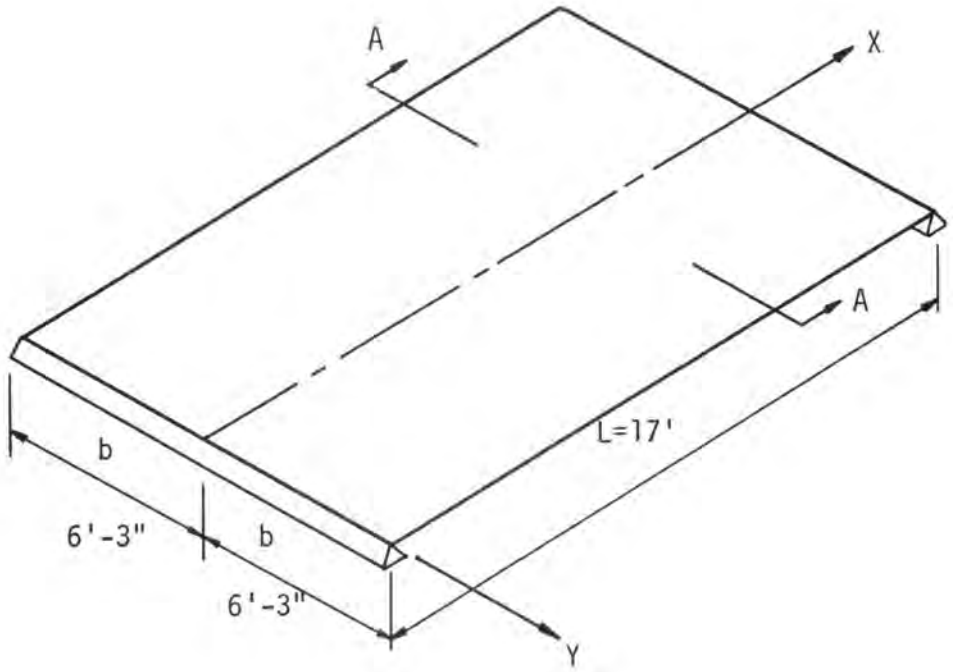

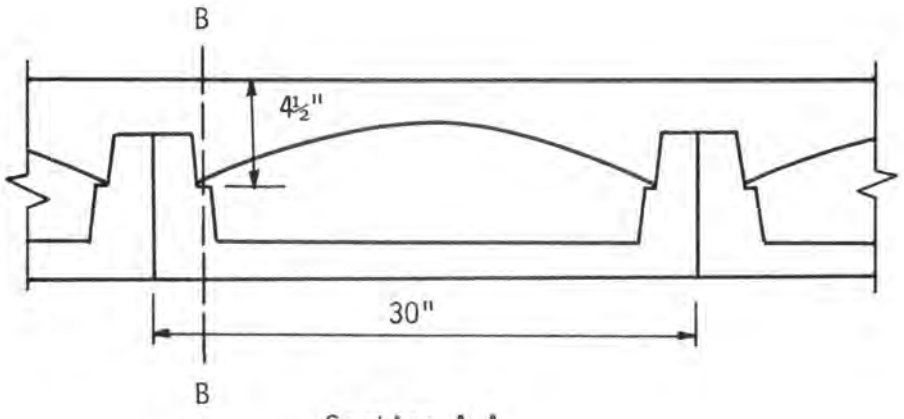

Section A-A

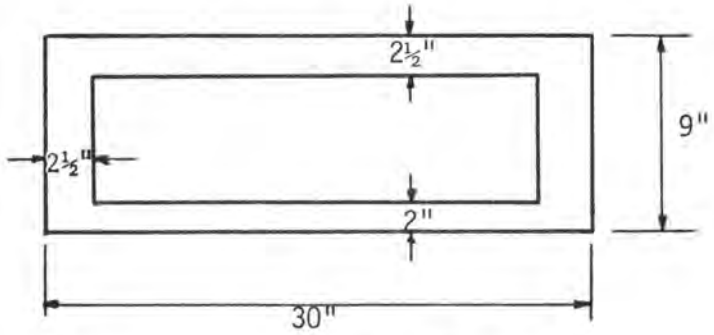

Simplified Box Section

Fig. A. 1 Model Bridge Dimensions

$$A = 25\ (4.5) = 112.5\ in^2$$

$$\oint \frac{ds}{t} = \frac{25}{2} + \frac{25}{2.5} + \frac{(4.5)(2)}{2.5} = 26.1$$

$$K = \frac{(4)(112.5)}{26.1} = 1939.6\ in^4$$

$$\gamma_x = \frac{GK}{b_1} = \frac{(2307)(1939.6)}{30} = 149.2 \times 10^3\ Kip - in.$$

in the y - direction: a one-foot strip

$$K = \frac{1}{2}\left(\frac{bt^3}{3}\right) = \frac{(12)(4.5)^3}{(2)(3)} = 182.25\ in^4$$

$$\gamma_y = \frac{Gk}{L_1} = \frac{(2117)(132.25)}{12} = 32.2 \times 10^3\ Kip - in.$$

Torsional Stiffness Parameter

$$\alpha = \frac{\gamma_x + \gamma_y}{2\sqrt{\rho_x \rho_y}} = \frac{(149.2 + 32.2)10^3}{2\sqrt{(33.9)(253.3)(10^6)}}$$

$$= \frac{181.4}{185} = 0.99$$

assume $\alpha = 1.0$, full torsion

Two sets of curves have been presented by Morice and Little[5], for the two cases of $\alpha = o$ and $\alpha = 1$. Fig. A.2 is a sample reproduction of these curves. As can be seen, the group of curves shown corresponds to the case where $\alpha = 1$, and load P is applied at various locations - b, -3b/4, .., + b. Each curve represents a particular location of load and is labled accordingly. However, the group of curves give the distribution coefficient, K, only for bridge location b/4 i.e., the fraction of the load transferred to point b/4, depending to position of the load.

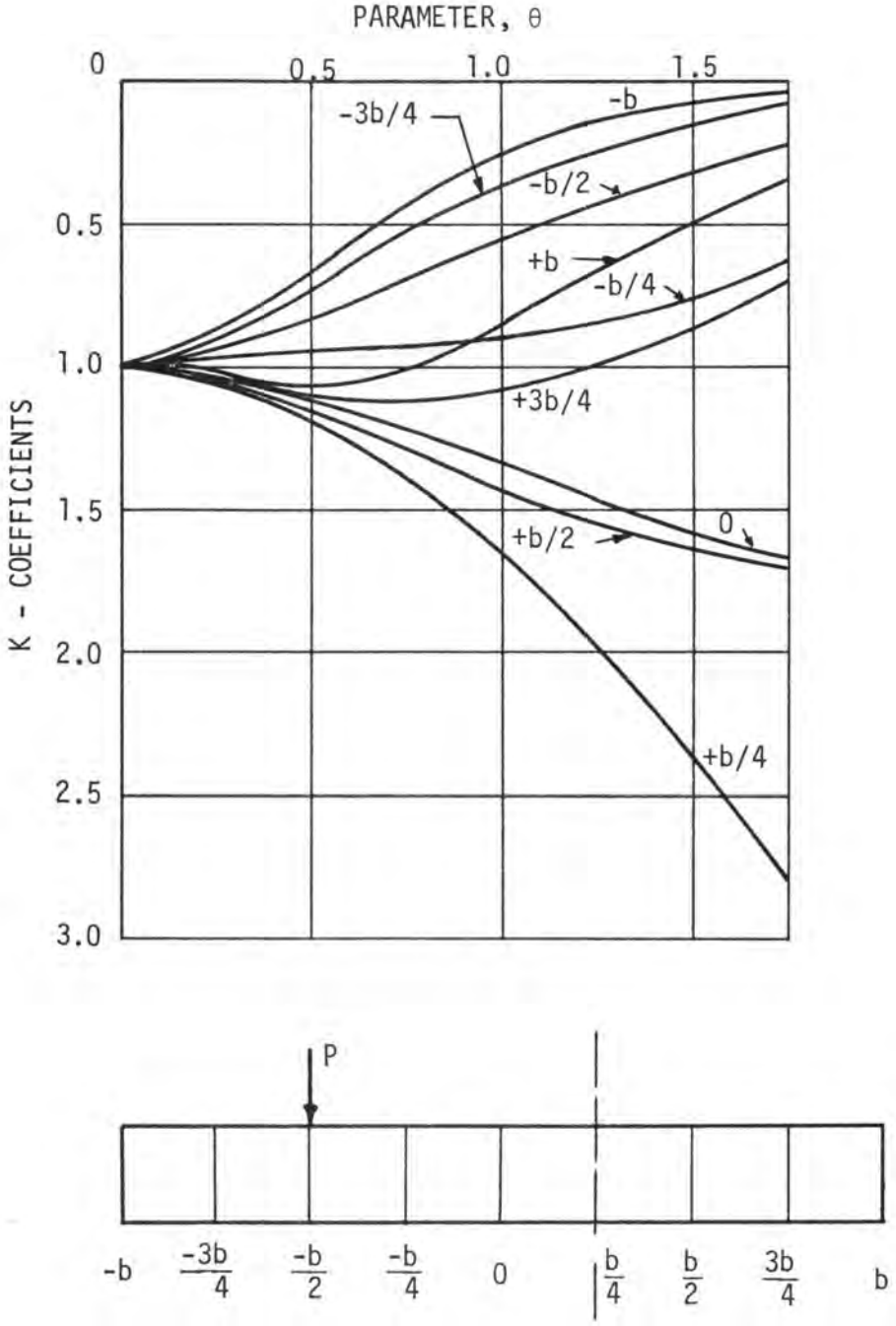

Fig. A.2 Full-Torsion K - Coefficient for Bridge Location b/4 Due to Moving Load P (Massonnet)

Given a particular value of θ. K coefficients can readily be obtained from the group of curves. Utilizing the Maxwell's reciprocal theorem, Fig. A.2 can be considered to represent the case where load is stationary at $\frac{b}{4}$ and each curve represent a certain bridge location. Applying this theorem, the curve labled $e = \frac{b}{4}$ in Fig. A.3 was obtained. In the same manner, the other curves in Fig. A.3 were plotted. These curves represent the K-coefficient influence line for the particular model bridge for load eccentricities $e = o, \ldots, e = b$. However, for this particular slab, the distribution coefficients for the center of the box members are of significance. For example, in Fig. A.3 the distribution coefficients, say for the exterior member, are the points of the intersection of the dashed lines (a) and (b) with the curves for positive and negative load eccentricities respectively.

Once again utilizing the reciprocal theorem one can consider that the position of the dashed line is the load position and the curves various locations on the bridge. Thus, Fig. A.4 was obtained for the three load positions shown.

It should be noted that for cases where α is between zero and one, K-coefficients should be obtained for $\alpha = o$ in the same manner as previously described and the following interpolation formula be used:

$$K_\alpha = K_o + (K_1 - K_o)\sqrt{\alpha}$$

where K_o and K, refer to cases $\alpha = o$, and $\alpha = 1$, respectively.

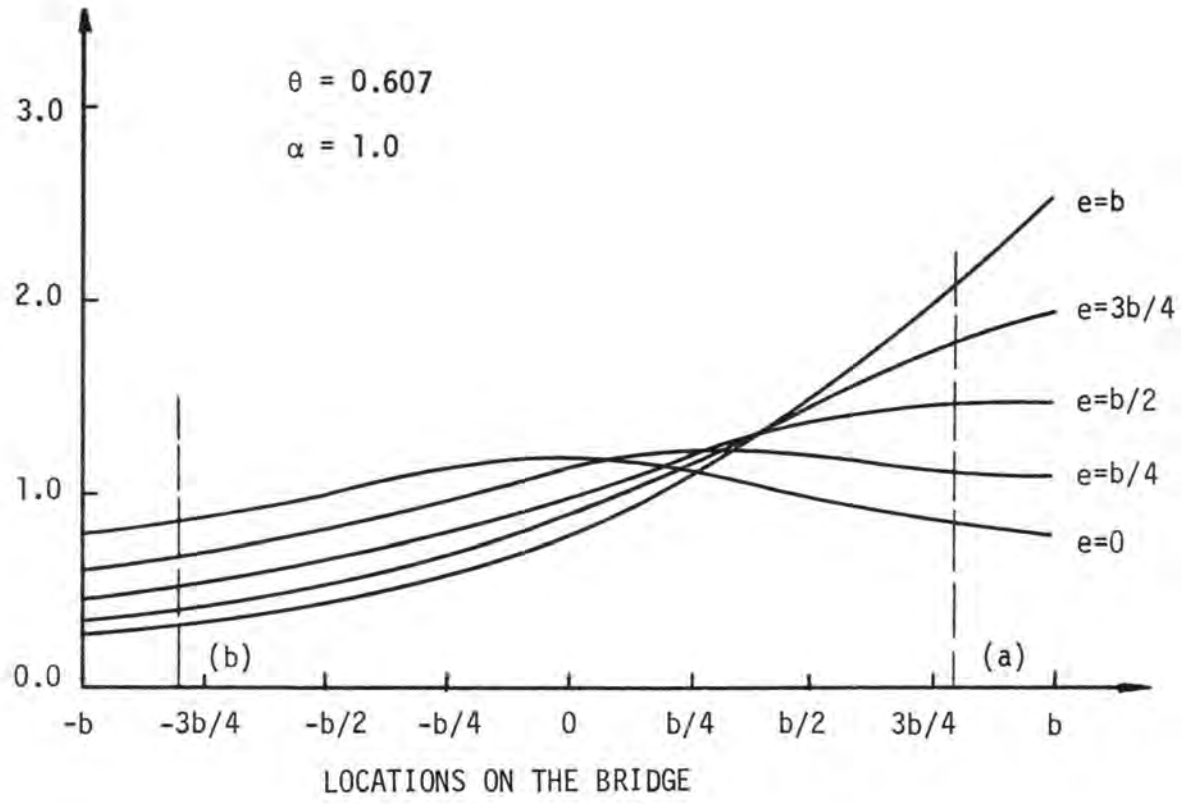

Fig. A.3 K - Coefficients for Various Locations on the Slab and Various Load Eccentricities, e

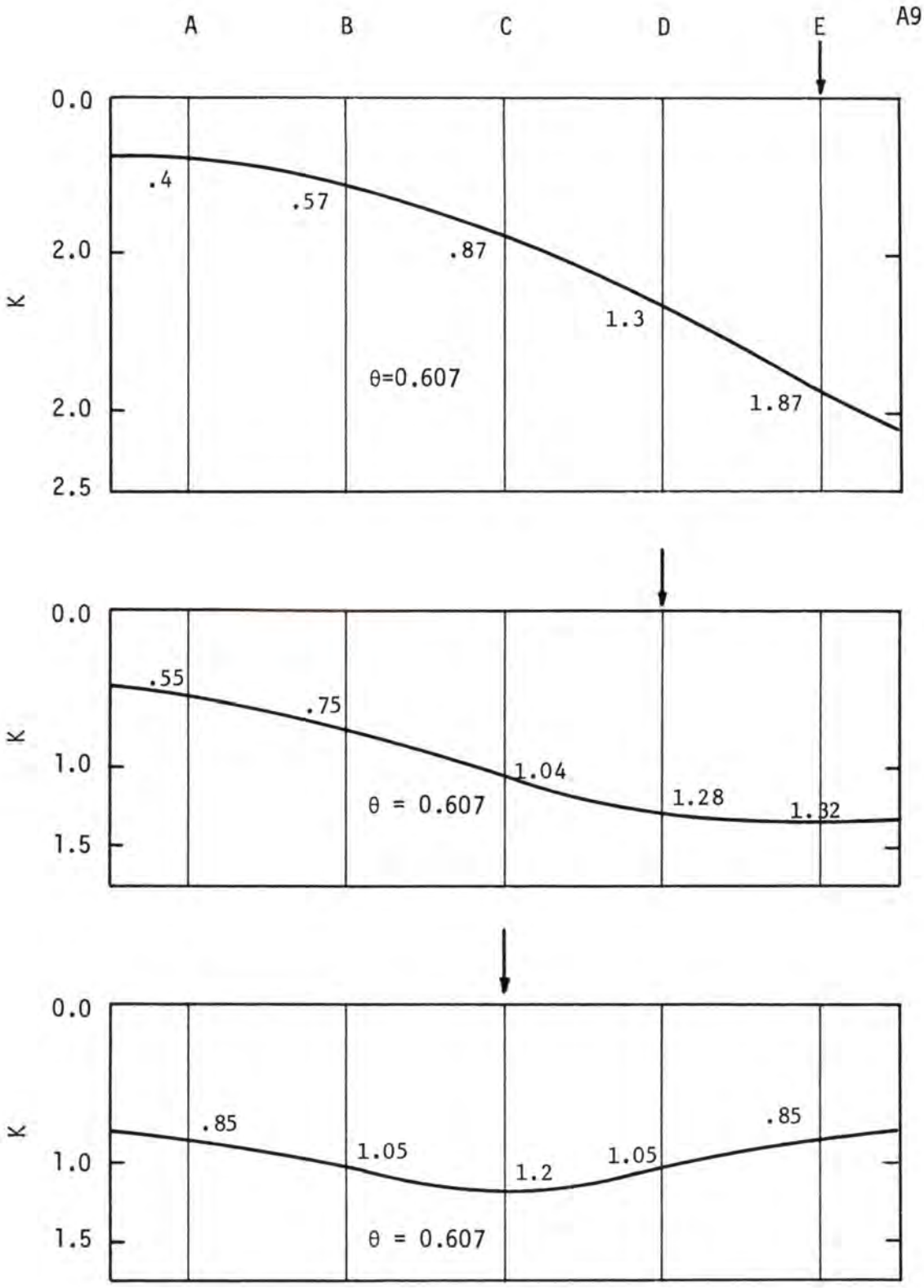

Fig. A.4 K - Coefficients Influence Line for Center of Box Members